INVESTIGATION OF NOVEL PKC TARGETS IN THE REGULATION OF AUTOPHAGY

by

HUMEYRA NUR KALELI

Submitted to the Graduate School of Engineering and Natural Sciences

in partial fulfillment of

the requirements for the degree of

Master of Science

Sabancı University

December 2019

INVESTIGATION OF NOVEL PKC TARGETS IN THE REGULATION OF AUTOPHAGY

APPROVED BY:

Assoc. Prof. Dr. Özlem Kutlu
(Thesis Supervisor) .....

Prof. Dr. Devrim Gözüaçık .....

Asst. Prof. Dr. Öznur Bayraktar .....

DATE OF APPROVAL: 06/12/2019

ABSTRACT

INVESTIGATION OF NOVEL PKC TARGETS IN THE REGULATION OF AUTOPHAGY

HUMEYRA NUR KALELI

Molecular Biology, Genetics and Bioengineering, M.Sc. Thesis, December 2019

Thesis Supervisor: Assoc. Prof. Ozlem Kutlu

Keywords: Autophagy, protein kinase C, Lentivirus transduction

Protein Kinase C (PKC) isozymes are serine/threonine kinases that are important for activation and/or inactivation of intracellular signaling pathways and therefore regulate cellular metabolism. Autophagy is a degradation mechanism functioning under basal conditions and activating under cellular stress including nutrient limitation, oxidative stress or abnormal protein accumulation. It is initiated by formation of double or multi-membrane vesicles in the cytoplasm. These vesicles engulf the cargo and carry it to the lysosome. After the fusion of autophagic vesicle with lysosomes, the cargo is degraded, and its constituents are recycled. The signaling pathways regulated by PKC isozymes are also involved in autophagy mechanism. However, the interaction between autophagy and PKC isozymes is still unclear. The aim of the study is to find novel proteins targeted by PKC isozymes during autophagy mechanism. For this aim, lentiviral shRNA library system was used for silencing of the genes in GFP-LC3 stably expressing mouse embryonic fibroblast (MEF) transgenic cells (MEF GFP-LC3). Upon activation of PKC isozymes, autophagic machinery was examined by GFP-LC3 puncta count, LC3 shift assay and p62 accumulation. Then the positive clones were selected, and their genomic DNA was isolated for target gene sequencing. The genes were identified with Sanger sequence analysis and their relationship with PKC isozymes were analyzed by using RT-q-PCR. Consequently, the role of target gene in the regulation of autophagy was determined by commonly used autophagy techniques.

ÖZET

OTOFAJİ DÜZENLENMESİNDE YENİ PKC HEDEFLERİNİN ARAŞTIRILMASI

HÜMEYRA NUR KALELİ

Moleküler Biyoloji, Genetik ve Biyomühendislik, Yüksek Lisans Tezi, 2019

Tez Danışmanı: Doç. Dr. Özlem Kutlu

Anahtar kelimeler: Otofaji, protein kinaz C, Lentivirus gen aktarımı

Protein Kinaz C (PKC) izozimleri, hücre içi sinyal yollarının aktivasyonunda ve/veya inaktivasyonununda önemli olan serin/treonin kinazlardır ve bu nedenle hücresel metabolizmayı düzenler. Otofaji bazal koşullar altında çalışan ve besin kıtlığı, oksidatif stres veya anormal protein birikimi dahil olmak üzere hücresel stres altında aktive olan bir öğütme mekanizmasıdır. Oluşumu sitoplazma içinde çift veya çok membranlı veziküller ile başlar. Bu veziküller kargoyu içine alır ve onu lizozoma taşır. Otofajik vezikülün lizozom ile birleşmesinden sonra, kargo öğütülür ve bileşenleri geri dönüştürülür. PKC izozimleri tarafından düzenlenen sinyal yolları ayrıca otofaji mekanizmasında da rol oynar. Buna rağmen, otofaji ve PKC izoenzimleri arasındaki ilişki hala belirsizdir. Bu çalışmanın amacı, otofaji mekanizması sırasında PKC izozimlerinin hedeflediği yeni proteinleri bulmaktır. Bu amaçla, GFP-LC3 proteinini stabil olarak eksprese eden fare embriyonik fibroblast (MEF) transgenik hücrelerinde (MEF GFP-LC3) lentiviral shRNA kütüphanesi gen susturmak için kullanılmıştır. PKC izozimlerinin aktifleşmesi ile, otofajik sistem GFP-LC3 nokta sayısı, LC3 değişim analizi ve p62 birikimi ile incelenmiştir. Daha sonra pozitif klonlar seçildi ve genomik DNA'ları hedef gen dizilimi için izole edildi. Genler Sanger dizi analizi ile tanımlandı ve bunların PKC izozimleri ile ilişkileri RT-q-PCR yöntemi kullanılarak analiz edildi. Sonuç olarak, hedef genin otofaji düzenlemesindeki rolü, yaygın olarak kullanılan otofaji teknikleri ile belirlendi.

“To my mother, father, and brother…”

“Canım anneme, babama ve kardeşime…”

ACKNOWLEDGEMENTS

I would like to express my sincere gratitude to my supervisor Assoc. Prof. Özlem Kutlu for her infinite support, guidance and motivation. I am grateful for her endless patience and encouragement. I realized her believe in me when I faced with several troubles during my research and she gave me every possible opportunity to improve my abilities in the project. It was a great opportunity to work under her supervision. I also thank to my master thesis committee, Prof. Devrim Gözüaçık and Assist. Prof. Öznur Bayraktar for spending their valuable time to evaluate my thesis and to provide valuable comments and advices.

I would like to express my special thanks to Özlem Yedier-Bayram and Seval Kılıç for their well-written journals, procedures and their endless help during my research. I was the only student when I participated in Kutlu Lab. Nevertheless, they always support me when I needed.

I would like to give grateful thanks to my lab members Ebru Özer and Veysel Oğulcan Kaya who have been also like sister and brother to me. I shared every moment in the lab with them and saved great memories especially during confocal experiments. It was really great to work with you guys! You never leave me alone when I do experiments in early mornings, late nights and weekends. I will keep listening Yaşar, Hatırla during cell culture experiments. I would also like to thank present members of Kutlu Lab for giving me valuable advices during preparation of my thesis. I especially thanks to Hale Kesim for her kindness and good faith.

I would like to thank my best friends Gözde Sert, Tuğba Türk and Ayşen Jale Endes who have been my friends and my family in Istanbul for 10 years. They have been always with me as true friend during my master and provide me funny, silly and lovely memories.

I would like to express my special thanks Dr. Yunus Akkoç, Dr. Nesibe Peker and Sinem Demirbağ for their endless support, friendship and their help on scientific matters. I would like to thank to my friends in the G168 Cell Culture Lab especially Elif Çelik and Ayhan Parlar who give experimental advices and share creative ideas. I would also like to express my thanks to Dr. Eray Metin Güler who is my friend and my first mentor during

my internships. Without his belief in me, I probably would not show courage to apply Masters in Sabancı University.

I would like to give my thanks to my first aid friends Melike Barak, Adnan Taşdemir and Dr. Mine Altunbek. They always helped me to find when I need any equipment or chemical during my stressful experiments. I shared very valuable moments with them in SUNUM and they made our office the best environment to work. I am very lucky to meet my friends that I always keep in touch.

I would like to express my thanks to TUBİTAK (The Scientific and Technological Research Council of Turkey) for financial support of my master project and me as master scholarship student. This project is supported by TUBİTAK-1001- The Scientific and Technological Research Projects Funding Program with Project No: 114Z836.

Finally, I would like to express my deepest appreciation to my mother, Sonnur Kaleli, my father, Süleyman Kaleli and my brother, M. Fatih Kaleli for their endless love and support. I am the prankish child of them, and I am sure they will be proud of me when they read these sentences. I love you and I am grateful to have you. Thank you for being wonderful family and thank you for your kindness and patience.

TABLE OF CONTENTS

LIST OF TABLES

LIST OF FIGURES

LIST OF SYMBOLS AND ABBREVIATIONS

α	Alpha
β	Beta
γ	Gamma
δ	Delta
ε	Epsilon
ζ	Zeta
η	Eta
θ	Theta
ι	Iota
κ	Kappa
λ	Lambda
μ	Micro
μL	Microliter
μM	Micromolar
AMPK	AMP activated protein kinases
ATG	Autophagy-related genes
Ca^{+2}	Calcium
CMA	Chaperone mediated autophagy
DAG	Diacylglycerol
DMEM	Dulbecco's modified eagle medium
DMSO	Dimethylsulfoxade
DPBS	Dulbecco's phosphate-buffered saline
EBSS	Earl's balanced salt solution
EDTA	Ethylenediaminetetraacetic acid
ER	Endoplasmic reticulum
FBS	Fetal Bovine Serum
GFP	Green Fluorescent Protein
HSP70	Heat Shock Protein 70
IP3	Inositol-1,4,5-Trisphosphate
JNK	C-Jun N-terminal kinase
LAMP2	Lysosomal membrane protein-2
LC3	Microtubule-associated protein 1 light chain 3
MAPK	Mitogen-activated protein kinases
MC	Monoclones including RFP-shRNA expression vector
mTOR	Mammalian target of rapamycin
NEAA	Non-essential Amino Acid
PDK1	Phosphatidylinositol-trisphosphate-dependent kinase
PE	Phosphotidylethanolamine
RFP	Red fluorescent protein

PI3K	Class-III-Phosphotidylinostiol-3-Kinase
PIP3	Phosphotidylinositol-3-phosphate
PKC	Protein kinase C
PMA	Phorbol 12-myristate 13-acetate
PS	Phophatidylserine
RAB23	RAB Oncogene Family Small GTP Binding Protein
RC	Monoclones including RFP control vector
ULK1	Unc-51 like autophagy activating kinase 1
TRPV6	Transient receptor potential cation channel subfamily V member 6

1. INTRODUCTION

1.1. Autophagy

The discovery of lysosomes by C. de Duve in the 1950s brings along crucial cellular system questions including what the fate across the regulation of lysosome is and how its regulation affects the protein- enzyme function (De Duve, Pressman, Gianetto, Wattiaux, & Appelmans, 1955). During the investigation of those questions, another research team, Marilyn Farquhar and her associates focused on electron microscopy images of cells and discovered the existence of several membrane-covered vesicles. Initially, they define them as lytic bodies, known as phagophore today. The vesicles engulfed mitochondria, ER and ribosomes are called autophagic bodies (Smith & Farquhar, 1966). Investigations have been accelerating and autophagosomes, autolysosomes, and even different types of autophagy mechanisms were discovered.

Autophagy is a well-conserved recycling mechanism in the cell to remove cellular waste and toxins in order to maintain energy homeostasis. The mechanism promotes survival by delaying senescence under stress conditions such as nutrient starvation or oxidative stress. In this mechanism, double-membrane vesicles surround non-functional organelles, protein aggregates, and cytoplasmic compartments and then these complexes transport toward lysosomes for degradation. Cooperation of different autophagy-related proteins known as ATG proteins maintain the autophagy stages, which include initiation, elongation, maturation, lysosomal fusion and degradation (Figure 2.) (Glick, Barth, & Macleod, 2010). Autophagy serves as a house cleaner because both unnecessary proteins and cellular organelles are swept to make room for newly built functional materials.

Insufficiency of autophagy results in disease progression due to the accumulation of waste materials (Levine & Kroemer, 2008).

mTOR mediated PI3K/Akt activation is well studied signaling pathway and negative regulation of mTOR pathway promotes formation of ULK1 complex with ATG proteins and initiates phagophore formation (Alers, Löffler, Wesselborg, & Stork, 2012; Jung, Ro, Cao, Otto, & Kim, 2010). Lipidation of LC3 results in the conversion of LC3-I to LC3-II protein that leads to the expansion of phagophore around recycling materials. Efficient fusion of autophagosome with lysosome creates autolysosome, where the waste materials are degraded (Nath et al., 2014).

Autophagy is classified into three main groups: Macroautophagy, microautophagy, and chaperone-mediated autophagy (CMA). In macroautophagy, larger molecules, such as organelles, protein aggregates that could not be degraded by the proteasomal system are recycled. In microautophagy, smaller molecules are directly transported to the lysosome and degraded. In chaperone-mediated autophagy, proteins having the KFERQ motif are first recognized by Heat Shock Protein 70 (HSP70) and then directed towards lysosome. These proteins are further identified by lysosomal membrane protein-2 (LAMP2) and engulfed in lysosomes for degradation.

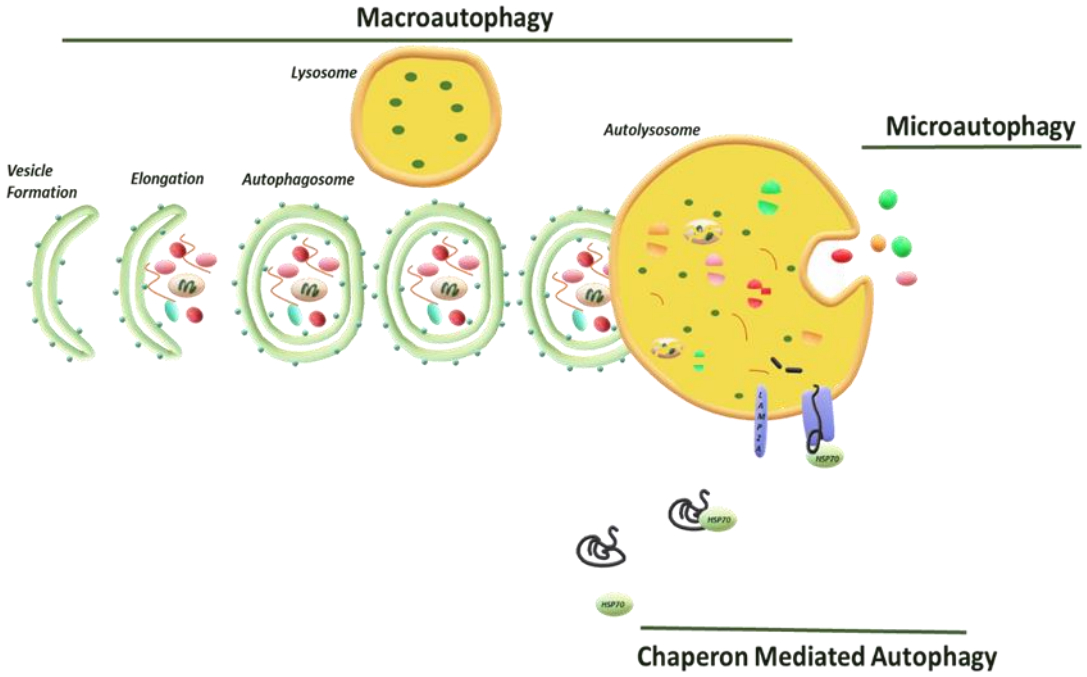

Figure 1.1. Illustration of autophagy mechanism

1.2. Type of Autophagy

1.2.1. Macroautophagy

Macroautophagy is the best characterized type of autophagy (Levine & Klionsky, 2017). Two main kinase systems known to regulate autophagy namely the mTOR–ULK1 and the BECN1 complex. In detail cell's energy sensor mTOR or TOR is an important kinase that regulates cell growth, proliferation, survival, death, and energy metabolism. It consists of two sets of proteins, mTORC1 and mTORC2. mTORC1 is involved in cellular events such as cell growth, proliferation, and death, while mTORC2 provides the regulation of the cellular skeleton. The mTORC1 protein cluster, which plays a role in autophagy activation in starvation conditions, consists of proteins called Raptor, mLST8, PRAS40, and DEPTOR, which bind to mTOR. When nutrient or growth factors are abundant, autophagy protein Ulk1 is phosphorylated by mTOR and this phosphorylation results in inactivation of autophagy. The ULK complex contains the ULK1 or ULK2 kinase, ATG13, FIP200 (focal adhesion kinase-family interacting protein of 200 kDa) and ATG101. However, when nutrients and growth factors are limiting in the environment or under ER stress, AMP-Kinase (AMP-activated kinase) activated by LKB1 (liver kinase B1) via the phosphorylation of the Raptor directly on the mTORC1 cluster. Alternatively, AMP-Kinase inhibits mTORC1 by blockade of Rheb (Ras-related small G protein) pathway via TSC2 inhibition in the upregulated signaling pathway of mTORC1. Thus, the formation of autophagosomes is triggered. When activated, mTORC1 favors cell growth by promoting translation via the phosphorylation of p70S6K (70 kDa polypeptide 1 ribosomal protein S6 kinase) and of 4E-BP1, an inhibitor of translation initiation, therein inactivating it (Y. Chen & Klionsky, 2011).

Another protein complex needed for the formation of autophagosomes is a complex of class III phosphatidylinositol 3-kinases (PI3K). The core components of PI3K complex are also responsible for the catalytic activity of the complex and these are VPS34 (vacuolar protein sorting 34), VPS15 and Beclin-1 (BECN1) proteins. PI3P plays a crucial role in the clustering of proteins required for autophagic vesicle formation in vesicle budding regions and provides a fusion platform for many proteins.

Phosphatidylinositol-3-phosphate (PI3P) constitutes an essential membrane component of the elongating isolation membrane and it is generated by VPS34 (Devereaux et al., 2013). In mammalian cells, PI3P molecules function as recruiting point for several autophagy-related proteins to the isolation membrane such as WIPI1/2, DFCP1, and Alfy. In addition to that, ATG9 (ATG9L1 in mammals) is also one of the crucial transmembrane proteins, plays a role in the lipid delivery and establishes a platform for recruiting effectors for the phagophore (Young et al., 2006).

The autophagic sac elongation involves two separate protein-protein interactions which resemble ubiquitination. The first pathway enables the binding of the ubiquitin-like ATG12 protein to ATG5 and then the ATG5-ATG12 complex recruits ATG16L to form the ATG12-ATG5-ATG16 complex. Here, the ATG7 and ATG10 proteins, which regulate the addition of ATG12 in a manner similar to ubiquitination, play the E1 and E2-like role, respectively (Hanada et al., 2007). The second pathway is the covalent binding of phosphatidylethanolamine (PE) to the protein LC3. LC3B protein is synthesized as precursor and is a critical component of autophagosome formation. During this formation, cysteine protease ATG4 cleaves LC3 from its C-terminus and a glycine residue is exposed. Cleaved form of LC3, is activated by ATG7 then transferred to ATG3 through covalent binding and linked to an amino group of phosphatidylethanolamines (PE). Conjugation of LC3-PE to both sides of the isolation membrane enables them to act as surface receptor for the specific recruitment of other proteins (Nakatogawa, Ichimura, & Ohsumi, 2007). The autophagosomal closure results in a typical double-membraned vacuole formation.

Apart from AMP-Kinase, PTEN which is one of the tumor suppressors converts PIP3 to PIP2 and inhibits mTOR via PI3K / Akt / TSC1-2 pathway so that has a role in autophagy regulation. Also, ERK1 / 2 and c-Jun N-terminal kinase1 (JNK1) in Ras / MAPK pathway have been found as inducers of autophagy (Obara, Noda, Niimi, & Ohsumi, 2008; Xie & Klionsky, 2007). Some of oncogenes such as Class I PI3K, Akt, TOR, Bcl-2 suppresses autophagy. Studies have shown that p53, one of the most important tumor suppressor genes, plays a dual role in autophagy (Pattingre & Levine, 2006; Tasdemir, Maiuri, Morselli, et al., 2008). A number of studies have shown that p53, particularly to the cell nucleus, induces autophagy dependent or independent of the effect of transcription (Levine & Abrams, 2008; Tasdemir, Maiuri, Galluzzi, et al., 2008). On the other hand,

some studies suggest that wild and mutant forms of p53 located in the cytoplasm suppress autophagy (Crighton et al., 2006; Feng, Zhang, Levine, & Jin, 2005). In addition, TNF-α (Tumor necrosis factor), which plays a fundamental role in many disease mechanisms, including cancer, has been shown to activate mTORC1 by phosphorylating the TSC1 complex (IKKβ) (Lee et al., 2007).

1.2.2. Microautophagy

Microautophagy involves direct engulfment of the proteins/cytoplasm into the lysosome (mammalians) or vacuole (plants and fungi) by invagination. Dynamin-related GTPase Vps1p plays an active role to regulate the invagination of microautophagic process. Importantly, these invaginations grow and shrink rapidly, and their frequency depends on the nutritional conditions. Starvation induces the initiation and extension of invagination respectively (Uttenweiler, Schwarz, & Mayer, 2005). During extension, this formation specializes into a characteristic tubular shape termed as "autophagic tube", depending on its unique structure and autophagy-related function (Müller et al., 2000).

The soluble substrates of microautophagy can be induced by N-starvation or rapamycin through the regulatory signaling complexes. The maintenance of organelle size, membrane homeostasis, and cell survival under N-restriction are considered as main functions of microautophagy (W.-w. Li, Li, & Bao, 2012). As a basic form of autophagy, microautophagy-dependent lysosomal/vacuolar degradative process is either non-selective or selective. The non-exclusive microautophagy engulfs soluble intracellular substrates by tubular invaginations. Thus, the selective microautophagy sequesters specific organelles with arm-like protrusions. The non-selective microautophagy is regularly observed in mammalian cells, while the three forms of selective microautophagy are frequently induced in yeasts (micropexophagy, piecemeal microautophagy of the nucleus (PMN), micromitophagy).

1.2.3. Chaperon mediated autophagy

Chaperone mediated autophagy (CMA) is a selective form of autophagy and it has a distinctive way to recognize cargo molecules. In CMA, well known chaperone protein heat shock protein 70 (hsp70) recognizes proteins with specific pentapeptide motif KFERQ and translocates them to the lysosomal lumen for degradation via lysosomal-associated membrane protein 2A (LAMP2A) (Kaushik & Cuervo, 2018). CMA activation is much crucial for some cellular events such as control of cell cycle (Park, Suh, & Cuervo, 2015), CD4+ T cell activation (Valdor et al., 2014), protein quality control (Schneider et al., 2015), and response to starvation (Finn & Dice, 2005). In addition, link between CMA mechanism and neurodegenerative diseases has been reported. It is known that, CMA contributes to the degradation of misfolded proteins, which prone to become aggregates.

1.2.4. Selective Autophagy

For cellular homeostasis, proper clearance of organelles or specific molecules is critical in living organisms. In selective autophagy, receptor proteins recognize specific cargo such as mitochondria, lipid droplets, invading pathogens etc. These receptor proteins are responsible for carrying the cargo to the site of autophagosomal engulfment. So far, several specific receptors or adaptor proteins, which regulate the selective degradation of specific cargo have been identified and partially characterized. Selective autophagy has drawn the attention of researchers because of its potential importance in clinical diseases; however, the physiological roles are not yet fully understood.

1.2.4.1. Mitophagy

Mitochondria are highly dynamic, double-membrane surrounded organelles, which have a major function in energy production within the eukaryotic cells. They are involved in a variety of cellular functions within eukaryotic cells and have an ancient bacterial origin. Besides energy production, they are involved in amino acid synthesis, fatty acid

production, heme synthesis, innate immunity (Tait & Green, 2012) as well as programmed cell death processes (Green & Kroemer, 2004).

Considering all these missions of mitochondria, to control its balance according to cell's demand is essential for disease progression. The selective degradation to remove damaged mitochondria by autophagy, is called mitophagy (K. Wang & Klionsky, 2011). Parkin and PINK1-dependent mitophagy is one of the best-studied forms of mitophagy (Matsuda et al., 2010; Narendra, Tanaka, Suen, & Youle, 2008). Mainly, mitophagy is maintained by these two famous genes and their loss-of-function mutations are linked to early-onset of Parkinson's Disease. PTEN-induced putative kinase 1 (PINK1), encodes for a mitochondrially localized kinase, and PARK2, encodes a cytosolic E3 ubiquitin ligase (Narendra et al., 2008). Under normal conditions, after being synthesized as a precursor in the cytoplasm, PINK1 is imported to mitochondria through translocase of the outer membrane (TOM) and translocase of the inner membrane (TIM) complexes. When PINK1 is imported, it is post-translationally modified within mitochondria by mitochondrial proteases. PINK1 is first cleaved through its N-terminal matrix targeting sequence (MTS) by matrix processing peptidases (MPP) and resulting cleavage followed by another cleavage by Presenilin-associated rhomboid-like protease (PARL) in the matrix (Deas et al., 2011). PARL-mediated N-terminal cleavage results in destabilizing Phe104 residue and therefore, when retranslocation from mitochondria to cytoplasm emerges, degrades by proteasome through recognition of its N-terminus (Yamano & Youle, 2013). Under stress conditions, PINK1 import to mitochondria is blocked, PINK1 proteins on OMM get dimerized and this dimerization is necessary for autophosphorylation events. This accumulated PINK1 phosphorylates various targets, including ubiquitin, and recruits the cytoplasmic E3 ubiquitin ligase, Parkin protein. After this moment, Parkin acts as an amplifier of the PINK1-generated mitophagy signal (Lazarou, Jin, Kane, & Youle, 2012).

Additionally, AMBRA1 is another key mitophagy regulator that allows proper Parkin-dependent and independent mitochondrial clearance. It is ubiquitously expressed in adult midbrain and found in complex with Parkin but AMBRA1 has no effect on Parkin recruitment to mitochondria, its activation effect on PI3K suggested to be critical for PINK/Parkin-mediated mitophagy (Strappazzon et al., 2015).

1.2.4.2. Lipophagy

Lipid droplets (LDs) are specialized organelles composed of lipids essential for cellular energy (metabolism) and membrane production (Walther & Farese, 2012). LDs consist of a neutral lipid namely triglyceride (TG) and cholesterol esters and are coated by a phospholipid monolayer and various proteins such as the perilipins (PLINs). Under certain conditions like nutrient deprivation, cellular lipids stored as triglycerides in LDs are hydrolyzed into fatty acids for energy. As expected second cellular response to starvation is the induction of autophagy. Interrelationship between autophagy and lipid metabolism was shown in mouse hepatocytes for first time in 2009 by Mochida et al. This study revealed that inhibition of macroautophagy, pharmacologically or by silencing of the ATG genes, leads to the accumulation of TGs and LDs in serum-starved hepatocytes. Thus, nutrient limitation triggers LD degradation by macroautophagy in hepatocytes (Mochida et al., 2015).

Microlipophagy has been detected in yeast in response to nitrogen starvation, glucose depletion, survival during stationary phase, and phospholipid imbalance. Under these conditions, LDs are taken up into the vacuole at sites of vacuolar membrane invagination (Seo et al., 2017; van Zutphen et al., 2014).

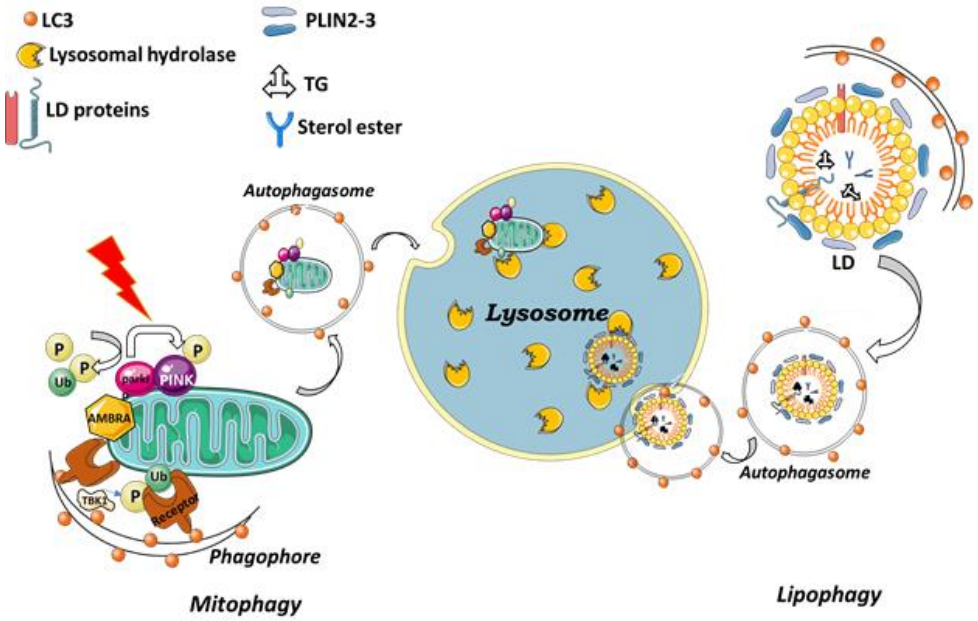

Figure 1.2. Illustration of selective autophagy mechanism

1.3. Protein Kinase C Family

Protein Kinase C (PKC) protein family is a phospholipid-dependent serine/threonine kinase that are discovered by Nishizuka and his colleagues in the 1970s. This protein family is initially defined as PKM due to their Mg^{+2} dependent activations, but later on, they are called as PKC due to their Ca^{+2} dependent activations. Protein kinase family consists of over 15 subgroups with more than 500 kinases, each of which is involved in the regulation of gene expression therefore, downregulation or upregulation of these kinases induces severe consequences in the progression of disorders such as cancer or neurodegenerative diseases.

Due to the regulatory role in cellular activities through interaction of other sig nalingproteins, PKCs have a critical role in disease progression. To date, the involvement of PKCs in disease progression is being studied in both in vitro and in vivo models as well as patient-derived samples. In vivo animal models were designed to analyze the development of cancer (Hafeez et al., 2011; Leitges, 2007; Spitaler & Cantrell, 2004), neurodegenerative diseases (W. M. Lau et al., 2018; Russo et al., 2018; Sanna, Quattrone, Ghelardini, & Galeotti, 2014), metabolic disorders (Jha et al., 2016; Sajan et al., 2018) and muscular defects (Madaro et al., 2012; Quack et al., 2011; G.-S. Wang et al., 2009).

1.3.1. Structure and Classification of PKC isozymes

Protein kinase C (PKC) is the subgroup of the kinase family and comprises ten members. The distinguishing feature of PKCs is that they include N-terminal regulatory domain connected to C- terminal catalytic domain through a hinge domain (K.-P. Huang, 1989; Newton, 1995). Each PKC isozymes has common structural characteristics since they have four conserved domains, C1, C2, C3 and C4. C1 and C2 locate on N-terminal regulatory domain while C3 and C4 reside on C-terminal catalytic domain. C1 domain is composed of 50 amino acid sequence and has C1A and C1B domains. Cysteine and histidine residues on C1 domain associate with zinc ions. Zn^{+2} association is important because of protection of the conservation of tertiary structure. C1 domain structure shows that it has hydrophilic ligand binding site enclosed with hydrophobic amino acids. On hydrophilic region, there are diacylglycerol (DAG) and phorbol esters binding sites (Schultz, Ling, & Larsson, 2004). When DAG and phorbol esters bind on that region, C1

domain becomes completely hydrophobic and this configuration enables C1 domain to translocate and bind to the membrane (Schultz et al., 2004). C1 domains are activated by different lipids and the situation causes difference in activation of some PKCs within same subgroup. C2 is consist of 130 amino acids which include secondary messenger, Ca^{+2}, binding site (Johnson, Giorgione, & Newton, 2000). Among protein kinases, sequences of C2 domain do not show homology and have diverse differences. Because of the differences, C2 domain has distinctive functions as protein phosphorylation or lipid modification. There are three Ca^{+2} binding sites on C2 domain facilitating interaction with phosphatidylserine at the membrane and resulting in conformational change of PKCs (Bolsover, Gomez-Fernandez, & Corbalan-Garcia, 2003; Edwards & Newton, 1997). C3 has ATP binding site and C4 has protein substrate binding sites (Ramos, Reyes-Reyes, & Nanez, 2018). All PKC isozyme has pseudo-substrate region that is a substrate-mimicking short amino acid sequence that binds the substrate-binding site in the catalytic domain, inhibiting the enzyme activity (Yang, Langston, Tang, Kiani, & Kilpatrick, 2019) In the latent form, the N-terminal pseudo-substrate (PS) region which is acting as autoinhibitory region on PKC renders the active site, which is located between the two lobes of the catalytic domain (Igumenova, 2015).

Based on structural features and activators, PKCs classify split into three categories. Conventional PKCs consist of PKCα, PKCβI, PKCβII, and PKCγ. Novel PKCs consist of PKCδ, PKC η, PKC θ, and PKC ε. Atypical PKCs consist of PKC ζ and PKC ι/λ (Steinberg, 2008).

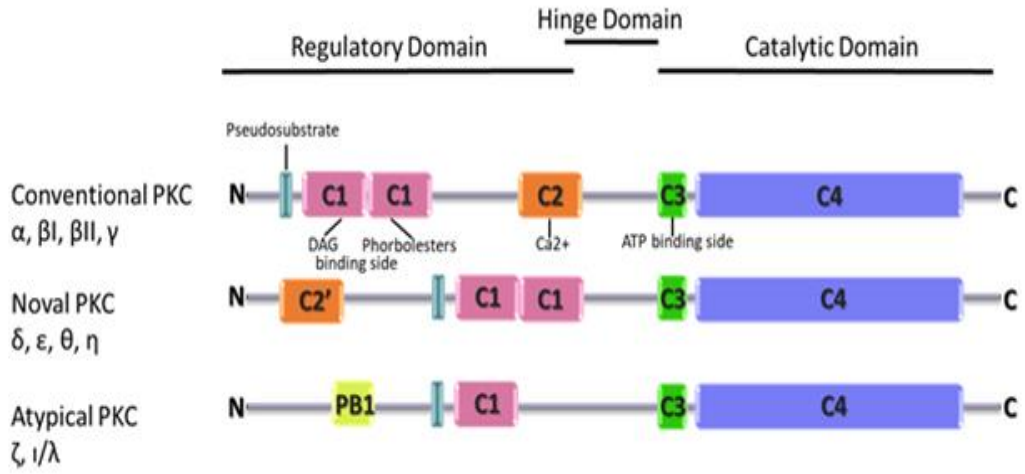

Figure 1.3 Domain structures of PKC isozymes.

1.3.2. Activation and Function of PKC isozymes

PKCs stay at the resting state without secondary messengers. Hydrolysis of phosphatidylinositol 4,5-bisphosphate (PIP2) leads to diacylglycerol (DAG) and inositol 1,4,5- trisphosphate (IP3) formation. IP3 translocates to ER and initiates intracellular Ca^{+2} release (Spitaler & Cantrell, 2004). This secondary messenger mobile to C2 domain of PKC and bind on "region". Binding of Ca^{+2} changes affinity of C2 domain for membrane. Conformational change and translocation to the membrane happen. When PKCs reach to membrane, they interact with PS to enable strong membrane penetration. Interaction with Ca^{+2} is not enough to activate conventional PKCs because they also need DAG and phorbol for activation. When DAG and phorbol esters bind to C1 domain, PKCs become active and stimulate downstream signaling pathways. Foremost, phosphatidylserine interacts with C1 domain and provide suitable circumstance for binding of DAG (Steinberg, 2008). When Ca^{+2}, DAG and phosphatidylserine collaborate, conformational change PKCs at membrane occurs in order to remove pseudo-substrate sequence. In comparison to conventional PKCs, novel PKCs do not require Ca^{+2} for activation by reason of their C2 domain sequence variation on Ca^{+2} binding site. So that their activation via Ca^{+2} does not proceed. Accordingly, novel PKCs only require DAG and PS for the initiation of signaling cascades. At last, atypical PKCs consist of PKC ζ and PKC ι/λ, which only need DAG for activation.

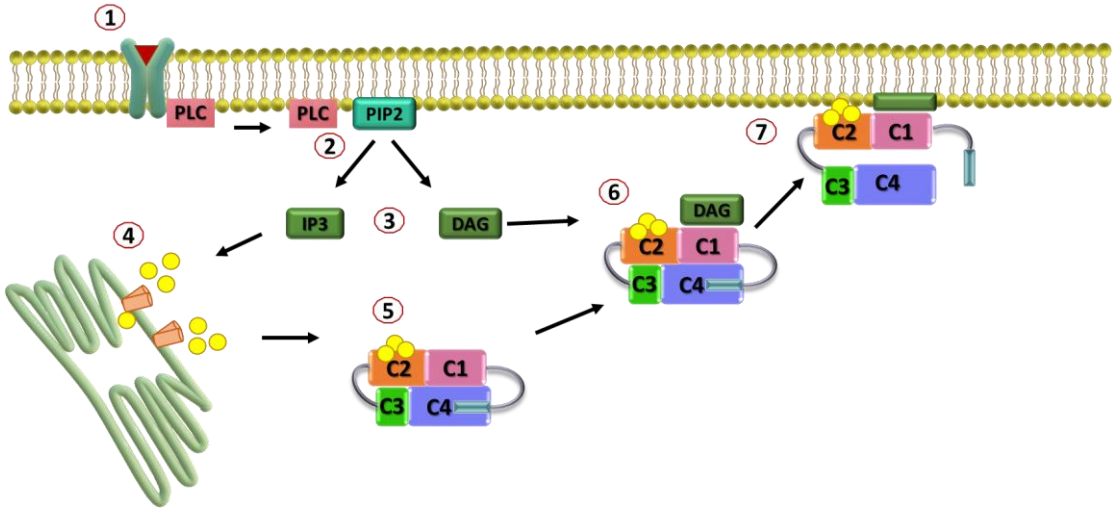

Figure 1.4 Activation of Protein Kinase C

1.3.3. PKC in Autophagy Mechanism

Activation of Protein kinase C isozymes is involved in extensive cellular mechanisms, including the autophagy pathway. Each isozyme has a diverse role in the pathway due to its phosphorylation abilities. Various functions of PKCs in main autophagy pathways such as PI3K / Akt / mTOR have been reported in several studies.

It has been described that, PKCα suppresses autophagy by inducing expression of miR-129-2 in maternal diabetes and provokes neural tube defects (F. Wang et al., 2017). In another study, tetrandrine, which is a PKCα inhibitor, causes autophagy induction in breast cancer cells through the AMPK independent and mTOR dependent mechanism (Wong et al., 2017). On the other hand, Xue et al. showed that the inhibition of PKCα causes lysosomal dysfunction and abnormalities in autophagosome-lysosome fusion in NRK-49F cells. Thus, the recovery of autophagic flux by PKCα activation resulted in kidney fibrosis through TGFβ-1 induction (Xue et al., 2018). Cisplatin, a chemotherapeutic agent, has a role for initiating several signaling pathways in order to activate cell death. The expression of PKCβ is promoted by cisplatin treatment in HeLa cells. When PKCβ is silenced, suppression of cisplatin-induced apoptosis was observed while formation of cisplatin-induced autophagy was promoted (N. Li & Zhang, 2017). Another drug, clozapine used in schizophrenia therapy, has a role in autophagy regulation. PKCβ restriction by ruboxistaurin increase clozapine-induced lipophagy and causes the recycling of lipid accumulation both in vitro and in vivo (Rimessi et al., 2017). Conventional PKCγ reduces neuron-specific autophagy via phosphorylation of mTOR on serine 2448 and serine 2481 (Hua et al., 2018). It has been reported that cPKCγ provokes the inhibition of ubiquitin C-terminal hydrolase L1 (UCHL1) and is involved in the ERK-mTOR mediated autophagy during ischemic neural injury (Dan Zhang et al., 2017).

Moreover, inhibition of PKCδ has a role in the correction of nephrotoxicity in kidneys by upregulating autophagy through blockage of cisplatin-induced mTOR, AKT, and ULK1 pathway (Dongshan Zhang et al., 2017b). Similarly, PKCδ was used to phosphorylate GSK3αβ and suppress autophagy under Cadmium-induced Heme oxygenase-1 (HO-1) expression (So & Oh, 2016). Inhibition of PI3K/Akt/mTOR pathway through PKCδ results in impairment of autophagic flux in neural retina cells (S.-P. Huang, Chien, & Tsai, 2015). PKCε has a role in lipid metabolism by participating in hepatocyte autophagy (Yan, Niu, & Tian, 2018). Reversely, PKCε suppresses autophagy in glioblastoma cells

(Toton et al., 2018). Another isozyme, PKCθ, activation in Epstein-Barr virus (EBV)-infected cells causes phosphorylation of p38 and MAPK where it leads to autophagy induction (Gonnella et al., 2015). Hypoxic-induced autophagy is enhanced under calcium-dependent PKCθ activation (Jin et al., 2016). Interestingly, under pathogenic infection, autophagy mechanism is upregulated due to an increase in the pathogen's phagosomal escape, and PKCη silencing results in suppression of ATG7, an essential protein in autophagosome formation. Even though ATG7 levels decreased in the absence of PKCη, the number of phagosomes is not changed. Therefore, PKCη in autophagy regulation may have indirect effects and is subjected for further research (Micheva-Viteva, Shou, Ganguly, Wu, & Hong-Geller, 2017).

PKCι downregulates autophagic flux by repressing LC3 conversion. Accordingly, PKCι knockdown resulted in autophagic degradation of Hsc70 through CMA independent degradation (B.-S. Wang et al., 2013). Also, downregulation of PKCι promotes autophagic degradation of β-catenin, independent of CMA (B.-S. Wang et al., 2014). In another study, PKCι knockdown induces autophagy via the restriction of PI3K/Akt/mTOR pathway. Overexpression of mutant PKCι protein induces autophagosome formation and depletion in p62 protein. So, they suggested that overexpression of mutant PKCs may be used as antagonists of wild type PKCι for the upregulation of autophagy (Qu et al., 2016).

2. AIM OF THE STUDY

In the literature, studies showed that some PKC isozymes have role in the regulation of autophagy; yet, the exact mechanism of the relationship between autophagy and PKC isozymes is still unclear. In this project, we aimed to find novel proteins targeted by PKC isozymes during autophagy mechanism by shRNA-based target gene screening.

3. MATERIALS

3.1. Cell Culture

Table 3.1 Cell Culture Solutions & Reagents

Cell Culture Reagents	**Supplier**
Dulbecco's Modifed Eagle's Medium	PAN Pan-P04-03500
Fetal Bovine Serum (FBS)	PAN P30-3304
Penicillin/Streptomycin (100X)	PAN-P06-07100
L-Glutamine	PAN P04-80100
1x MEM Non-Essential Aminoacid	Gibco 11140-35
EBSS	Biological Industries BI02-010-1A
Lipofectamine 2000	Invitrogen 11668-19
Trypsin-EDTA (0.5 mM EDTA, 0.025% Trypsin)	PAN P10-019100
Phosphate Buffer Saline	PAN PAN-P04-036503
FuGENE 6	Promega E2691
PEI	Polysciences, Inc. 23966
Opti-MEM	Gibco 31985-047
G-418	Roche 04727894001

3.2. Plasmids for Transfection

Table 3.2 List of Plasmid

Plasmids	Supplier
PKCδ	Addgene
shPKCδ	Addgene
siTRPV6	Dharmacon SO-2747429G
pCDNA3.1	Addgene
pMAX-GFP	Lonza vpd-1001
psPAX2	Addgene12260
pMD2.G	Addgene12259
pRSI9-U6-(sh)-UbiC-TagRFP-2A-Puro	Addgene 28289
DECIPHER Lentiviral shRNA Library MM1	Addgene 28287

3.3. Antibodies for Immunouorescence and Western Blotting

Table 3.3 List of Antibodies

Antibody	Company
Actin	Sigma A5441
SQSTM1	BD Transduct Lab 610832
LC3	Sigma 7543
TRPV6	Alomone Lab A036
PKC δ	Santa Cruz sc213
Secondary anti-mouse	ImmunoResearch Lab 115035003
Secondary anti-rabbit	ImmunoResearch Lab 111035144

3.4. General Kits

Table 3.4 List of Kits

Kit	Company
QIAquick PCR purification kit	QIAGEN 28704
ECL	Roche 1201520001

NucleoBondTM Xtra Midi Plus	Macherey-Nagel 740420
SYBR Green	Roche 04887352001
Genomic DNA Isolation Kit	QIAGEN 69504
Amaxa Nucleofector™ Kits for Human Dermal Fibroblast (NHDF)	Lonza vpd-1001

3.5. Chemicals and Reagents

Table 3.5 Chemicals & Reagents

12	**Brand**
2-Mercaptoethanol	Neofroxx 1414
2-Propanol	Neofroxx 1496
LB Broth Agar	Caisson Labs LBP03
Agarose	Sigma A9539
Albumin Fraction V (Bovine Serum Albumin, BSA)	Sigma A3059
Ammonium persulfate (APS)	Neofroxx 1610
Ampicillin	Neofroxx 1728GR010
Bradford Reagent	Sigma B6916
Bromophenol blue	PanReac Applichem A3640
Calcium chloride-dihydrate	Merck A1229282
Ceramide	Santa Cruz Sc3527
Chloroform	Sigma C2432
DMSO	Sigma D2650
dNTP-Mix, 20mM	GeneOn
Ethanol	InterLAB
Ethylene diamine tetra acetate (EDTA)	Neofroxx 1108
50bp DNA Ladder	New England BioLabs N3236S
Glycerol	Neofroxx 1280LT001
Glycine	Neofroxx 1154
HCl	Sigma 7102
HEPES	Sigma H6147
Methanol	InterLAB
Kanamycin	Neofroxx 1162gr010
Milk powder	Neofroxx 1172
Nonidet P40	Applichem A1694
Nitrocellulose Membrane	Milipore IPVH00010
Nuclease free water	Roche 03315843001

PageRuler Prestained Protein Ladder	ThermoFisher 26616
Paraformaldehyde	Sigma 158127
PMA	Milipore 524400
PMSF	Sigma P7626
Potassium chloride	Neofroxx 1197
Protease Inhibitors	Sigma P8340
RNase Inhibitor	ThermoFisher EO0382
SDS	Neofroxx 3250
Sodium Azide	Riedel de Haen 13412
Sodium chloride	Neofroxx 1236
Tetramethylethylenediamine (TEMED)	Sigma T7024
Tris (tris-hydroxymethyl-aminomethane)	Sigma T1503
GENEzol RNA Isolation Reagent	Geneaid GZR100
Tween 20	Neofroxx 8506
Dream Taq DNA polymerase	ThermoFisher EP0701
DNase I	ThermoFisher EN0521
Revertaid reverse transcriptase	ThermoFisher EP0441
Random hexamer	ThermoFisher SO142
Ribolock RNase	ThermoFisher EO0381
PVDF WB Membrane	Roche 03010040001
RNase Exitus Plus	Applichem A7153

3.6. Buffers and Solutions

Table 3.6 Preparation of Buffer and Solutions

Buffer/Solution	**Component**
RIPA Buffer	25mM Tris 125 mM NaCl 1% NP40 0.5% Sodium deoxycolate 0.1% SDS 0.004% sodium azide pH 8.0
4XProtein Loading Dye	200mM TrisHCl pH 6.8 8% SDS 50% Glycerol 4% mercaptoethanol 50 mM EDTA 0.08% Bromophenol Blue

15% Seperating Gel	375 mM TrisHCl pH 8.8 0.1% SDS 15% Acrylamide:Bisacrylamide 0.05% APS 0.005% TEMED
10% Seperating Gel	375 mM TrisHCl pH 8.8 0.1% SDS 10% Acrylamide:Bisacrylamide 0.05% APS 0.005% TEMED
4% Stacking Gel	0.125 mM TrisHCl pH 6.8 0.1% SDS 4% Acrylamide:Bisacrylamide 0.05% APS 0.0075% TEMED
PBST	3.2 mM Na2HPO4 0,5 mM KH2PO4 1,3 mM KCl 135 mM NaCl 0,05% Tween 20 pH 7.4
2xHBS	140 mM NaCl 1,5 mM Na2HPO4 50 mM HEPES
4% Paraformaldehyde (PFA)	150 mM NaCl 1% NP40 0.5% Sodiumdeoxycolate 0.1% SDS 50 mM Tris pH 7.4
Red Solution	5% BSA, 0.02% Sodium Azide in PBST Phenol red pH 7.5
3X protein loading dye	6% SDS 30% Glycerol 16% β-Mercaptoethanol 0.1% Bromophenol blue in 1 M Tris-HCl pH 6.8
ECL solution	25 mM luminol 9 mM coumeric acid, 70 mM Tris-HCl pH 8.8
50X TAE	2M Tris 0.5M EDTA 1M Glycial Acetic Acid ddH_2O up to 1 lt

3.7. Software and Websites

Table 3.7 List of Software and Websites

Name	Purpose
ImageJ	Image analysis
http://www.ensembl.org/index.html	Genome sequence analysis
https://www.uniprot.org/	Genome sequence analysis
https://primer3plus.com/	Primer design program
https://www.addgene.org/	Vector map analysis
GPS 2.0	Phosphorylation Site Identification
Phosphomotif	Phosphorylation Site Identification
DISPHOS	Phosphorylation Site Identification
KinasePhos2.0	Phosphorylation Site Identification
NetPhos 3.1	Phosphorylation Site Identification
NetPhorest	Phosphorylation Site Identification
PKIS	Phosphorylation Site Identification
PhosphoPick	Phosphorylation Site Identification
Muside	Phosphorylation Site Identification

4. METHODS

4.1. Cell Culture

Mouse embryonic fibroblast (MEF) GFP-LC3 transgenic cells and HeLa cells stably expressing LC3 were maintained in Dulbeco's modified Eagle's medium (DMEM) supplemented with 10% (v/v) heat-inactivated fetal bovine serum, 100 U/ml penicillin/streptomycin, 2 mM L-glutamine and 1x MEM non-essential amino acid solution. For MEF GFP-LC3 single cell monoclones, puromycin (3µg/ml) was added into complete medium. For HeLa GFP-LC3 stable cells, G-418 (0,6mg7ml) was added into complete medium. Cells were maintained at 37^0C with 5% CO_2. Starvation induced autophagy was established by treatment of cells with Earl's balanced salt solution (EBSS) for 2 hours. PMA (100nM) and ceramide (1µM) treatments were performed for 30 minutes.

For cryopreservation of cells, cells in 10cm culture dishes were detached with trypsin and counted. Each cryopreservation tubes contained at least 1,5 million of cells. Cryotubes were prepared with 900 µl cell suspension and 100 µl DMSO. Cryotubes including cells were froze in cryobox including isopropanol and stored at -80^{o}C overnight. Next day, cryotubes were transferred to liquid nitrogen tank for long term preservation.

For cell thawing, cells preserved into nitrogen tank were taken and thawed into 37^{o}C water bath for 15 seconds. Then they were transferred into 15 ml falcon tube including 5 ml complete medium. Cell suspension was centrifuged at 300g for 5 minutes and pellet was dissolved into 8 ml complete medium and seed in 10 cm culture plate.

4.2. Decipher Lentiviral shRNA library Transduction

DECIPHER lentiviral shRNA library, Mouse Module 1: Pathway Targets comprises 27,000 shRNAs targeting 5,000 gene sequences and carries a puromycin-resistance cassette. Calcium- phosphate transfection method was used for transduction of lentiviral shRNA library. HEK293T cells were transduced with 10 µg lentivirus vector, 8 µg psPAX2 and 2 µg pmD2.G in DMEM containing 10%FBS, 2mM L-Glutamine and 100U/ml penicillin/streptomycin. Total volume of plasmid mixture was completed to 225 µl with Hyclone water and 25 µl 2.5 M CaCl2 was added. This mixture was added onto 250 µl of 2xHBS dropwise. 8 hours later, cells were washed with 1X PBS three times, and fresh media was added. After 24 hours, media containing lentiviruses were collected and fresh media were added. 36 hours later, media were harvested again and combined with the previously collected media and centrifuged at 300 × g for 5 minutes. Supernatant was filtered with 0,45 µm filter, aliquoted and stored at -80 °C. MEF GFP-LC3 transgenic cells were infected with 100 µl of the lentiviral supernatant. 6 hours later, cells were washed, and fresh media were added. After 72 hours, transduction efficiency was checked under an Olympus inverted microscope. Transduced cells were selected with 3 µg/mL puromycin for 10 days. Single cell colonies were produced.

4.3. Target Gene Sequencing

4.3.1. Genomic DNA Isolation

Genomic DNA was isolated by QIAamp® DNA Mini Kit as described by the manufacturer. Briefly, MEF GFP-LC3 transgenic monoclones were seeded on 10cm cell culture dishes (2x 10^6 cells/dish) and cultured at 37^0C with 5% CO_2. Next day DMEM was aspirated and cells were rinsed with 2 ml 1X PBS. For harvest cells, 2 ml 1X PBS were put on culture dish and gently scraped with using cell scraper. Cell suspension were collected in 15 ml centrifugation tube and centrifuged at 300 × g for 5 minutes at room temperature (15–25°C). Supernatant was aspirated and cells were resuspended in 200 µl 1X PBS. They were transferred into 1,5 ml microcentrifuge tube. 20 µl QIAGEN proteinase K was added and vortexed. 200 µl Buffer AL was added to the suspension and

mixed by up&down and vortexed for 15 seconds. The susspension were incubated at 56^0C for 10 minutes. After incubation, 200 µl ethanol was added and vortexed for 15 seconds. Then the mixture was transferred to mini spin column and centrifuged at 6000 × g for 1 minute at room temperature. The column was located on new 2 ml collection tube. 500 µl Buffer AW1 was added and centrifuged at 6000 × g for 1 minute at room temperature. The column was located on new 2 ml collection tube. 500 µl Buffer AW2 was added and centrifuged at 14000 × rpm for 3 minute at room temperature. The column was located on new 1.5 ml microcentrifuge tube and centrifuged at 15000 × rpm for 1 minute in order to eliminate remaining buffer. The column was located on new 1.5 ml microcentrifuge tube and 50 µl Buffer AE was added into the column. The sample was incubated at room temperature for 5 minutes then centrifuged at 6000 × g for 1 minute. Concentration of the genomic DNA was measured using Thermo Fisher 2000 NanoDrop spectrophotometer. The sample was stored at $+4^0$C for further use.

4.3.2. shRNA-specific Barcode PCR Amplification

To determine shRNA barcodes in monoclones, PCR performed with primer sets designed to amplify the barcode sides on genomic DNA of the samples (Table 4.1). Each 25 µl reaction included 50 ng gDNA of monoclones,10 µM dNTP, 0.5 µM primers, Taq polymerase, Taq polimeraz bufer and nuclease free water.

Table 4.1 PCR reaction Primers

Primer Name	Sequence
FwdHTS	5’-TTCTCTGGCAAGCAAAAGACGGCATA-3’
FwdU6-1	5’-CAAGGCTGTTAGAGAGATAATTGGAA-3’
FwdU6-2	5’-CCTAGTACAAAATACGTGACGTAGAA-3’
RevcPPT-5	5’-TGCCATTTGTCTCGAGGTCGAGAA-3’
RevHTS1	5’-TAGCCAACGCATCGCACAAGCCA-3’

Table 4.2 PCR reaction Reagents

Reaction Reagents	**Amount (µl)**
10X Taq polymerase buffer	2,5
Forward primer	1
Reverse primer	1
dNTP (10 µM)	0,5
gDNA 50ng	Determined to each gDNA
Taq polymerase	0,25
Nuclease-free Water	Up to 25 µl

PCR was performed at 95^0C for 1 minute followed by 30 cycles of 95^0C 30 minutes, 55^0C 30 minutes, 72°C 30 minutes. Final polymerase step was performed at 72°C 3 minutes. PCR products were stored at $+4^0$C for further use.

Table 4.3 PCR reaction for Barcode amplification

	Cycle	Time	Temperature °C
Initial Denaturation	1	1 minute	95
Amplification	30	30 seconds	95
		30 seconds	55
		30 seconds	72
Final polymerase	1	3 minutes	72

4.3.3. Agarose Gel Electrophoresis

1 gram of agarose powder was mixed with 50 ml 1X TAE buffer in a 100 ml microwavable flask for the preparation of 2% agarose gel. The flask was then placed into

the microwave until the agarose powder disolved completely in the buffer. The solution then left at room temperature for cooling. Mixture was poured carefully without making bubbles into a clean gel tray and comb was placed on the tray. Gel was stayed to dry for 20-30 minutes at room temperature. After the gel began to polimeraze, it solidified. Dried gel was placed in the electrophoresis tank filled with 1X TAE buffer. 20 µl samples were prepared by mixing 4 µl 6X DNA loading dye. In first well, molecular weight DNA ladder was loaded and each sample were loaded. The gel was run at 100 Volt constant voltage for 30 minutes. After running, the gel was placed and incubated for 20 minutes into 100 ml 1X TAE buffer containing 5 µl of ethidium bromide. After EtBr incubation, the gel was rinsed with water. DNA bands were visualized under UV-light.

4.3.4. Purification of PCR Products

PCR products were run on 2% agarose gel and the fragments were visualized under low exposed UV-light. DNA fragments were isolated from the gel by using bistoury. The isolated fragment was weighted in 1.5 ml microcentrifuge tubes. DNA fragments were purified by using QIAquick PCR purification kit according to the manufacturer's *instructions*. Briefly, 200 µl Bufer NTI was added in the tube containing DNA fragment and incubated at 50 ^{0}C for 10 minutes. The mixture was vortexed each 3 minutes. QIAquick PCR purification kit column was placed in 2 ml collection tubes.Then melted gel sample was transferred into columns and centrifuged at 11000 × g for 30 seconds for DNA binding on silica membrane. 700 µl Buffer NT3 was added to the column for cleaning of the membrane. The liquid collected in the tube was discarded and column was centrifuged one more time at 11000 × g for 1 minute in order to eliminate remaining buffer. Then column was placed on clean 1.5 ml microcentrifuge tube. 20 µl Buffer NE was added and the column was incubated 1 minute at room temperature. Then the column was centrifuged at 11000 × g for 1 minutes. Concentration of the purified DNA was measured by using ThermoFisher 2000 NanoDrop spectrophotometer. Samples were sent to BMLabosis (Turkey) for Sanger sequence analysis.

4.3.5. Target Gene Identification

DECIPHER^{TM} barcoded shRNA library, Mouse Module 1 (Cellecta): Pathway Targets, includes 27,500 shRNAs with 4,625 genes. Manufacturer provides a document including

target mRNA RefSeq# and HUGO gene symbol. Barcode sequences were searched at the document included HUGO Gene Symbol and RefSeq.

Cellecta DECIPHER shRNA Library
Mouse Module 1
Signaling Pathway Targets
4,625 Targets, 27,500 shRNA
Cat.# DMPAC-M1-P
shRNA and barcode Sequences
Module Identifier: AT (AT in HT sequencing)
v1a, 2/14/14
(for pRSI9 and pRSI12)

HT Sequencing QC in pRSI12: 3/5/12

gene#	gi	RefSeq	HUGO Gene Symbol	CDS/ UTR	sense	sense + mismatches	18-nt barcode
2032	62909982	NM_001013391.1	Cpsf6	CDS	CTGGTGATTATGGGAGTGC	CTGGTGATTgTGGGAGTGt	CAGTGTGTGTGTGTGTCA
2032	62909982	NM_001013391.1	Cpsf6	CDS	GAAATCTAACATGGTGGAC	GAAATCTAACATGGTGGAt	TGGTGTGTGTGTGTGTAC
2967	118130112	NM_011580.3	Thbs1	CDS	CTGTAGGTTATGATGAGTT	CTGTAGGTTATGATGAGTT	ACGTGTGTGTGTGTGTTG
1398	31982067	NM_009015.2	Rad54l	CDS	GTCCATTAAGAAGCGAGCC	GTCCATTAAGAAGtGAGCt	CAGTGTGTGTGTGTCAGT
3309	121583921	NM_031156.2	Ide	CDS	CCTGGTCATTATCTTGGTC	CCTGGTCATTATCTTGGTt	ACGTGTGTGTGTGTCACA
4313	145966832	NM_007891.3	E2f1	CDS	CATCCAGCTCATTGCCAAG	CATCCAGCTtATTGCtAAG	GTGTGTGTGTGTGTCAAC
1637	34996508	NM_194350.1	Maf	CDS	CAAGGAGAAATACGAGAAG	CAAGGAGAAATAtGAGAAG	TGGTGTGTGTGTGTCATG
1637	34996508	NM_194350.1	Maf	CDS	ACAAGGAGAAATACGAGAA	ACAAGGAGAAATAtGAGAA	ACGTGTGTGTGTGTACGT

Figure 4.1. Cellecta Decipher shRNA Library document. Barcode sequence site was highlighted and indicated with an arrow.

4.4. Measurement of Targets' mRNA level by RT-q-PCR

4.4.1. RNA Isolation

In order to determine the amount of TRPV6 and RAB23 mRNA level in monoclones RNA isolation was applied as following. MEF GFP-LC3 monoclones were seeded in 6 well culture plates as $1x10^6$ cell/well. Next day cells were treated with 0.006% DMSO as vehicle control and 100nm PMA for 30 minutes, EBSS and EBSS with 100nm PMA for 2 hours. After the treatment procedure, cells were washed with 2 ml 1X PBS. RNA extraction was conducted by using Genezol RNA isolation reagent. 1 ml Genezol RNA reagent was put on the cells for lyses and incubated for 5 minutes at room temperature. Cell lysate was collected into 1,5 ml microcentrifuge tube and 200 µl chloroform was added. The mixture was up&down for 15 seconds to mix homogenously. The color change was observed from pink to pale pinkish after mixing. The solution was incubated 15 minutes at room temperature. After incubation, the tube was centrifuged at 12000 × g for 10 minutes at room temperature. The phase separation was observed respectively

upper colorless, middle white line and bottom pink. The upper phase was carefully transferred into clean 1,5 ml microcentrifuge tube with avoiding touch to white phase. 500 µl ice-cold 2-isopropanol was added on the colorless phase and incubated on ice for 15 minutes. After incubation, the tube was centrifuged at 12000 × g for 10 minutes at $+4^0$C. Then supernatant was discarded, and 1 ml 75% ethanol was added onto the pellet. The mixture was centrifuged at 12000 × g for 10 minutes at $+4^0$C. Supernatant was discarded, and the pellet was incubated at room temperature for 20-30 minutes in order to eliminate ethanol. RNA pellets were dissolved in RNase free water by gently pipettage. Concentration of the RNA samples was measured using Thermo Fisher 2000 NanoDrop spectrophotometer and stored at -80 ^{0}C for further use.

4.4.2. cDNA Synthesis

cDNA was synthesized from 1000 ng RNA samples by reverse transcription PCR. First Dnase cycle was applied at 37^0C for 30 minutes. Then, EDTA cycle was applied for 75^0C for 10 minutes. Then, 10 µl PCR master mix including 5X reaction buffer, 10 mM dNTP, random hexamer (10 ng/µl), ribolock (40U/ µl), RT enzyme (200U/ µl) , nuclease-free water were added to EDTA cycle product. The cycles at 25 °C 10 minutes, 37 °C 60 minutes and 70 °C 10 minutes were applied 3 times. At the end of cycles, PCR reaction was stoped by incubating PCR products on ice for 1-2 minutes. The samples were stored at -20 ^{0}C for further analysis. The reagents and the process for cDNA synyhesis are stated as tables at the below.

Table 4.4 DNase Cycle Reagents

Reagents	**Amount (µl)**
1000 ng RNA	7
10X DNase I Buffer	1
DNase I enzyme	1

Table 4.5 EDTA Cycle Reagents

Reagents	Amount (µl)
DNase cycle product	9
25 mM EDTA	1

Table 4.6 Reverse transcription PCR (RT-PCR) Reagents

Reagents	Amount (µl)
EDTA cycle product	10
Nuclease-free Water	3,2
5X reaction buffer	4
10 mM dNTP	0,5
Random hexamer (10 ng/µl)	0,2
Ribolock (40U/ µl)	0,2
RT enzyme	0,1

4.4.3. RT-q-PCR

mRNA expression level of target genes upon PMA and starvation treatment was analyzed with Quantitative Real-Time PCR reaction. cDNA samples were diluted 1:5 ratio with PCR grade water and 5 µl of the dilution was used as templete in RT-qPCT analysis. 0,5 µl 10 µM forward and 0.5 µl 10 µM reverse primers, 4 µl water and 10 µl 2x Sybr Green was added in a well of white 96 well plate on ice with dark condition. The 96 well plate was sealed with colorles sealer and centrifuged at 1500 × g for 2 minutes. β-glyceraldehyde 3-fosfat dehydrogenase (GAPDH) was houskeeping gene used as control. The reaction began with

1 cycle preincubation at 95 °C for 10 minutes and followed 50 cycle amplification at 95 °C for 10 secs, 60 °C for 1 minute and 72°C for 10 seconds, 1 cycle melting curve at 95 °C for 5 seconds, 55 °C for 1 minute and 97 °C continuous and 1 cycle cooling at 40 °C for 30 seconds. Results were analysed by ΔΔCT method.

Table 4.7 List of RT-qPCR Primers

Primer Name	**Sequence**
Mouse Forward TRPV6	5′- TTGGGCTGGTGCAATGTCA-3′
Mouse Reverse TRPV6	5′-AGCCAGCAGAATCGCATCAAG-3′
Mouse Forward RAB23	5′-AAAATGAGGAAGCGGAGGGA-3′
Mouse Reverse RAB23	5′-AGTGACTTCTGACCGATGCA-3′
Mouse Forward GAPDH	5′-TCACCACCATGGAGAAGGC-3′
Mouse Reverse GAPDH	5′- GCTAAGCAGTTGGTGGTGCA-3′

Table 4.8 RT-q-PCR Reagents

Reagents	**Amount (µl)**
1:5 diluted cDNA	5
10 µM Forward Primer	0,5
10 µM Reverse Primer	0,5
PCR Grade Water	4
2x Sybr Green Master Mix	10

Table 4.9 RT-q-PCR reaction

Cycle	Time	Temperature °C
Pre-incubation	1	95
Amplification	50	95
		60
		72
Melting Curve	1	95
		55
		97
Cooling	1	40

4.5. LC3 Dot Analysis

HeLa LC3 stable cells were seeded on coverslips in the 6 well-plates as 1,25 x 10^5 cell/well and MEF GFP-LC3 transgenic cells were seeded in 12 well-plates as 2 x 10^4 cell/well. After 36 hours, corresponding wells were treated with EBSS for 2 hours. In the last 30 minutes of EBSS, 100 nM PMA and the necessary amount of DMSO were added to the media. Cells were fixed with 4% paraformaldehyde for 20 minutes on ice and mounted on the slides. Minimum 100 cells were counted for each sample under 60x magnification on Olympus BX60 fluorescence microscope and thresholds were determined as > 20 dots for HeLa LC3 stable cells and > 8 dots for MEF GFP-LC3 transgenic cells, respectively. Threshold number of LC3 puncta were determined in vehicle control group. Cells having LC3 puncta more than threshold number were counted as positive autophagic cells and cells having LC3 puncta less than threshold number were counted as negative autophagic cells.

4.6. Cell Lysate Preparation and Immunoblotting

Cells were lysed with RIPA buffer containing 1% complete protease inhibitors and 1 mM PMSF. The lysed was incubated on ice for 20 minutes and every 5 minutes it was mixed by vortexing. Then the lysed was centrifuged for 15 minutes at 13200 rpm, 4^0C. After centrifugation, the supernatant was taken into new tube and protein concentration was determined by Bradford Assay. For immunoblotting, 40 µg proteins were denatered in 3X protein loading dye for 10 minutes at 95^0C. Denatured proteins were loaded to the SDS-Polyacrylamide (PAGE) gels (Table 4.11 and 4.12) and separated using 15% gel for LC3 and 10% gel for other proteins. Proteins were transferred to nitrocellulose membranes at 250 mA for 1 hour for LC3 and 1 hours 15 minutes for other proteins. Membranes were blocked in 5% non-fat milk in PBS-T for 1 hour at room temperature and washed with PBS. Then membranes were incubated with primary antibodies diluted in red solution with 1:1000 ratio for 1 hour at room temperature or overnight at 4^0C then washed with PBS-T three times at each 5 minutes. After washing, the membranes were incubated with secondary antibodies prepared in 5% non-fat milk solution with 1:10000 ratio for 1 hour at room temperature and rinsed with PBS-T three times at each 5 minutes. Then membrane was placed on cassettes and signals were displayed by chemiluminescence reagent or homemade ECL solution. After observing signals, films were placed on membranes and the cassettes were closed and stored in dark for at least 20 minutes. Then the films were developed and fixed by using developer and fixer solutions until the bands arise. The band intensities were analyzed with ImageJ software.

Table 4.10 SDS- PAGE Separating gel preparation

Lower Gel	**15%**			**10%**		
	5 ml	10 ml	20 ml	5 ml	10 ml	20 ml
ddH_2O	850 µl	1.75 ml	3.5 ml	1.7 ml	3.4 ml	6.8 ml
50 % Glycerol	400 µl	750 µl	1.5 ml	400 µl	750 µl	1.5 ml
Lower Buffer	1.25 ml	2.5 ml	5ml	1.25 ml	2.5 ml	5ml
Bis/Acrylamide	2.5 ml	5 ml	10 ml	1.65 ml	3.35 ml	6.7 ml

10% APS	50 µl	100 µl	200µl	50 µl	100 µl	200µl
Temed	5 µl	10 µl	20µl	5 µl	10 µl	20µl

Table 4.11 SDS- PAGE Stacking gel preparation

Upper Gel	**2.5 ml**	**5 ml**	**7.5 ml**	**12.5 ml**
ddH_2O	1.62 ml	3.25 ml	4.88 ml	8.13 ml
Upper Buffer	625 µl	1.25 ml	1.87 ml	3.12 ml
Bis/Acrylamide	250 µl	500 µl	750 µl	1.25 ml
10% APS	20 µl	40 µl	60 µl	100 µl
Temed	5 µl	10 µl	15 µl	25 µl

4.7. Prediction of Protein-Protein Interaction of Target Protein and PKC by Bioinformatics-Based Software

Based on the findings indicating the presence of interaction between TRPV6 or RAB23 with PKCs, a preliminary analysis based entirely on amino acid sequence information was performed to give an idea of the regions through which this interaction could be achieved. For this purpose, bioinformatics tools, GPS 2.0, Phosphomotif, DISPHOS, KinasePhos2.0, NetPhos 3.1, NetPhorest, PKIS, PhosphoPick, and Muside, were used.

4.8. HeLa Cell Line Transfection Protocols

4.8.1. Transfection with Calcium-Phosphate

HeLa cells were seeded to 6-well plates as 150 000 cell/well. Next day, cells were transfected with 4 µg of pcDNA3.1 for control, pMAX GFP for transfection control by using Calcium-Phosphate Transfection. The total volume of plasmid mixture was completed to 54 µl with Hyclone water and 6 µl 2.5 M CaCl2 was added. This mixture was added onto 60 µl of 2xHBS drop by drop with continuous vortex. After 20 minutes of incubation, the solution was distributed to well as 120 µl. 8 hours after post transfection, cells were washed with 1x PBS twice and 2 ml complete medium added.

4.8.2. Amaxa Nucleofactor Transfection

HeLa cells are homogenized and counted with Trypan blue. 225 000 cell/well were transfered to eppendorfs and centrifuged at 3000 × g for 5 minutes Nucleofactor reagents were mixed with 4.5:1 nucleofactor to supplement ratio. Supernatant was discarded and cells were resuspended in 90 µL nucleofactor mixture including 4 ug pMAX GFP. Mixture is taken to cuvette and electroporated with AMAXA machine. After incubation for 10 minutes, cells were mixed with medium. Then they were seeded to 6 well plates. 8 hours after post transfection, cells were washed with 1x PBS twice and 2 ml complete medium added.

4.8.3. Lipofectamine Transfection

HeLa cells were seeded to 6-well plates as 125 000 cell/well. Next day, cells were transfected with 6 µg of pcDNA3.1 for control or pMAX GFP for transfection control by using Lipofectamine 2000. 6 µg of plasmids were mixed with 100 µL OptiMEM separately. The optimum ratio of DNA to Lipofectamine is ½ for HeLa cells. In another eppendorf tube, 12 µL Lipofectamine was mixed with 200 µL OptiMEM. The solutions were allowed for incubation for 5 min at RT. Then mixture with DNA were added on top of tube including Lipofectamine-OptiMEM. The solution was vortexed and incubated for 15 minutes at RT and vortexed each 5 minutes. During incubation process, cells were washed with 1X PBS once. After washing, 800 µL OptiMEM were given to each well. After incubation, Lipofectamine-plasmid solution was added to wells. After 4 hours from

post transfection, cells were washed with 1X PBS twice then 2 mL complete medium added.

4.8.4. Polyethyleneimine Transfection

HeLa cells were seeded to 6-well plates as 125 000 cell/well. Next day, cells were transfected with 4 μg of pcDNA3.1 for control or pMAX GFP for transfection control by using PEI. In one tube, 100 μL only DMEM mixed with 9 μL PEI. In another tube, 100 μL only DMEM mixed with 4 μg plasmid DNA. Then PEI-DMEM mixture was added drop by drop into plasmid-DMEM mixture on vortex. The solution was incubated for 15 minutes at RT. Cells were washed with 1X PBS ones and 2 ml complete medium added. After incubation solution was given to cells and 8 hours later the cells were washed with 1X PBS twice and complete medium added.

4.8.5. FuGENE Transfection

FuGENE 6 Transfection Reagent was used according to the manufacturer's *instructions.* Briefly, HeLa cells were split in 6-well plates as 150000 cells/well. Next day, FuGENE transfection was performed with 4 μg of pcDNA3.1 as control and pMAX-GFP for transfection control. In microcentrifuge tubes, pcDNA3.1 or pMAX-GFP was mixed with 90 μl OptiMEM then FuGENE 6 reagent was added to DNA-OptiMEM mixture as 3:1 ratio (FuGENE 6 Reagent (μl): DNA (μg)). The transfection reagent with DNA mixture was vortexed and incubated for 15 minutes at room temperature. Media of the cells was replaced with OptiMEM. After incubation, the mixture was given to cells drop by drop. 8 hours later, the cells were washed with 1X PBS and fresh media was added.

4.9. Flow Cytometry

For transfection efficiency check, flow cytometry protocol was applied. The cells were washed with 1X PBS and detached with trypsin. Detached cells were resuspended in 1 ml PBS including 10% FBS and centrifuged at 300 g for 5 minutes. Then pellets were resuspended in 200 μl PBS including 10% FBS and transferred into FACS tubes.

Cells were analysed with BD FACSCanto II flow cytometry system with green laser. Flourescence measurements were blank corrected with the fluorescence signals of non-transfected cells (20000 cells/ flow) and normalized with the same number of cells.

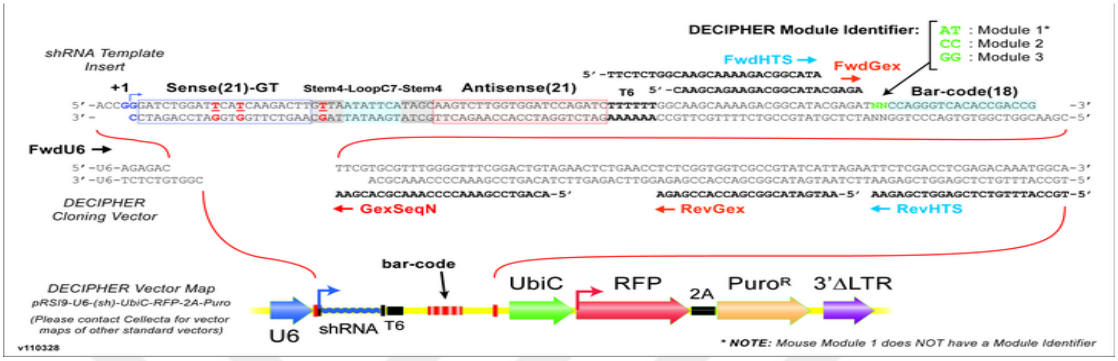

Figure 4.2. Representation of target gene including barcode sequence and shRNA region

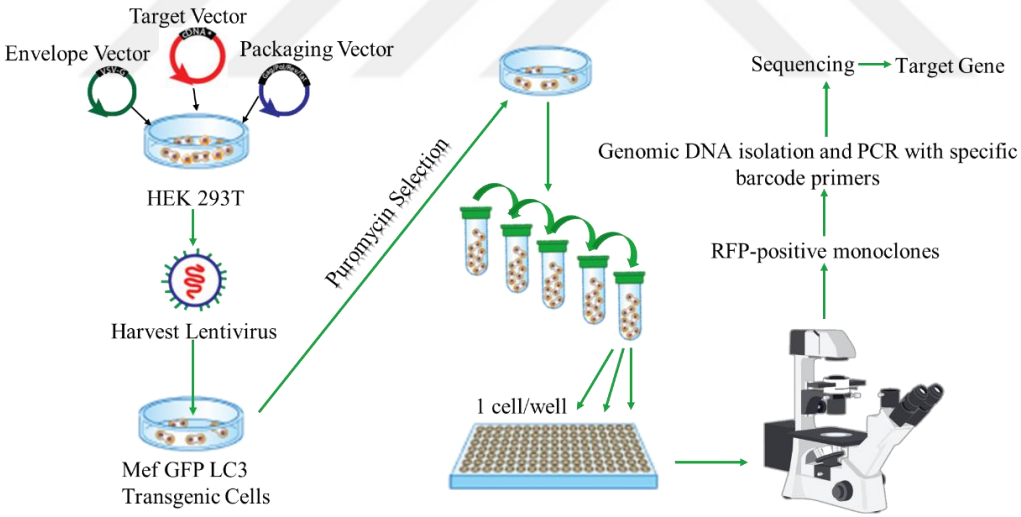

Figure 4.3. Lentivirus transduction and singe cell monoclone production

5. RESULTS

5.1. Autophagy is inhibited by PMA treatment in MEF GFP-LC3 cells

PMA is a synthetic drug that has structural and functional similarities with diacyl glycerol. Because of these characteristics, it is generally used as an activator of novel PKC isozymes in molecular biology. Previously, we showed that the stimulation of PKC isozymes by PMA treatment causes an alteration in autophagy regulation compared to basal condition. In order to confirm the effect of PMA in autophagy, we performed GFP-LC3 analysis.

GFP-LC3 dot counting is common technique used for visualization of autophagy activation under different conditions. Green dots in the cytosol represent the autophagosome-associated LC3-II formation. When MEF GFP-LC3 transgenic cells were treated with PMA, the number of GFP-LC3 dot formation was decreased compared to control group. Under starvation condition, autophagy is upregulated in order to maintain cellular homeostasis. The number of LC3-II dots was higher in starved cells, while lower in PMA group compared to control. The effect of PMA was confirmed by combined treatment with starvation media. PMA with starvation showed significant decrease in the number of LC3 puncta compared to starvation. Accordingly, autophagy activation is suppressed under PMA exposure in MEF GFP-LC3 cells, both in basal and starvation-induced conditions.

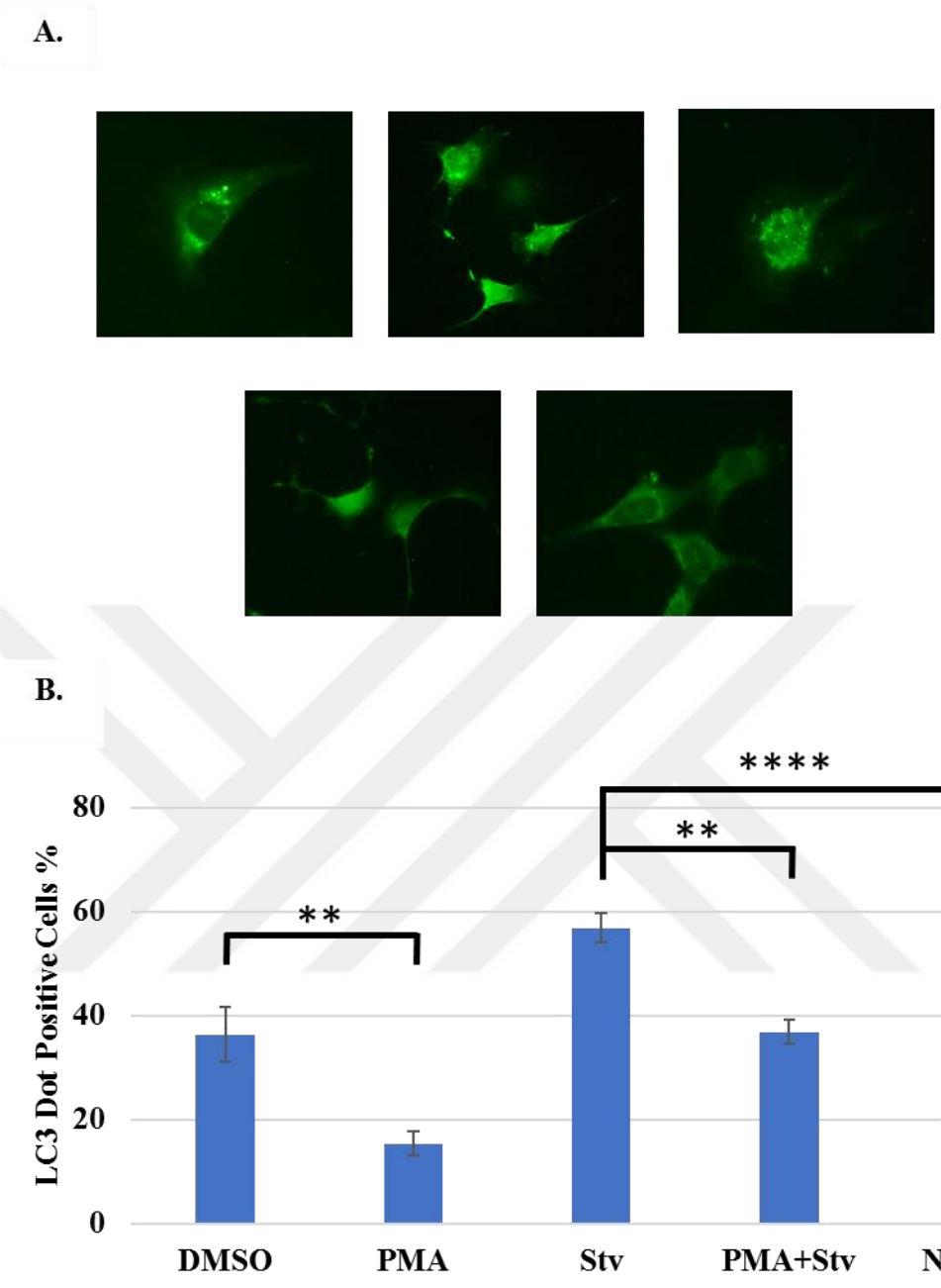

Figure 5.1. GFP-LC3 dot formation upon PMA and starvation treatment. (A.) Cells were treated with DMSO or PMA (100 nM) for 30 minutes and EBSS for 2 hours. Microscopic images were visualized under fluorescence microscopy with 60x objective (B.) Quantification of GFP-LC3 positive cells. Percentage of positive cells in total counted cells (minimum 100 cells) were compared in the graph. DMSO was used as a vehicle control of PMA. Data were shown as mean ± SD of independent experiments, n=3. *p<0.05, **p<0.01, ***p<0.001, ****p<0.0001.

5.2. Autophagy is induced by PKC activation with Ceramide treatment in MEF GFP-LC3 cells

Ceramide is commonly used as a secondary messenger in order to activate atypical PKCζ. Previously, we found that the atypical PKCζ promotes autophagy. In order to confirm previous data we performed autophagy analysis. Upon 1 μM Ceramide treatment for 30 minutes, the number of LC3 dots were increased in basal condition.

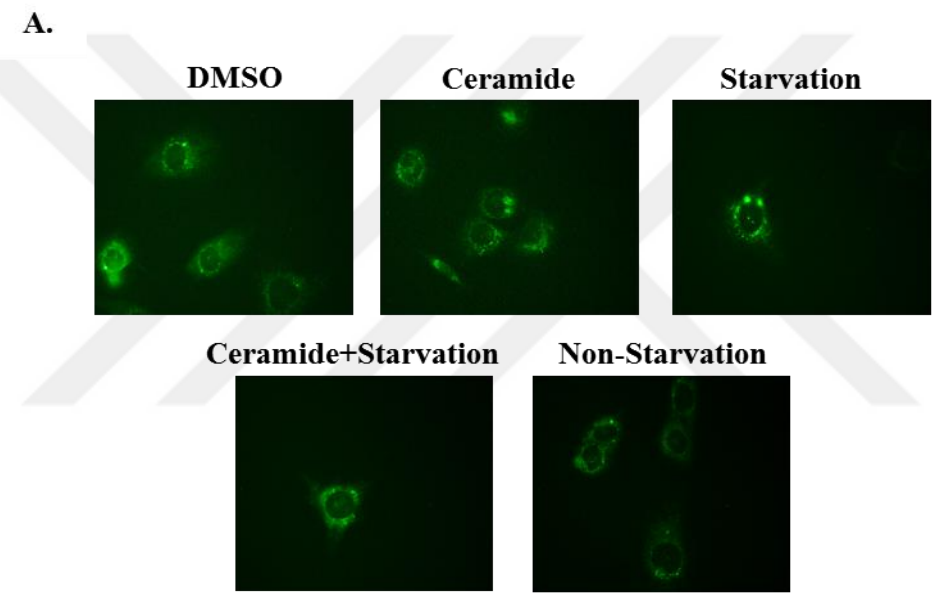

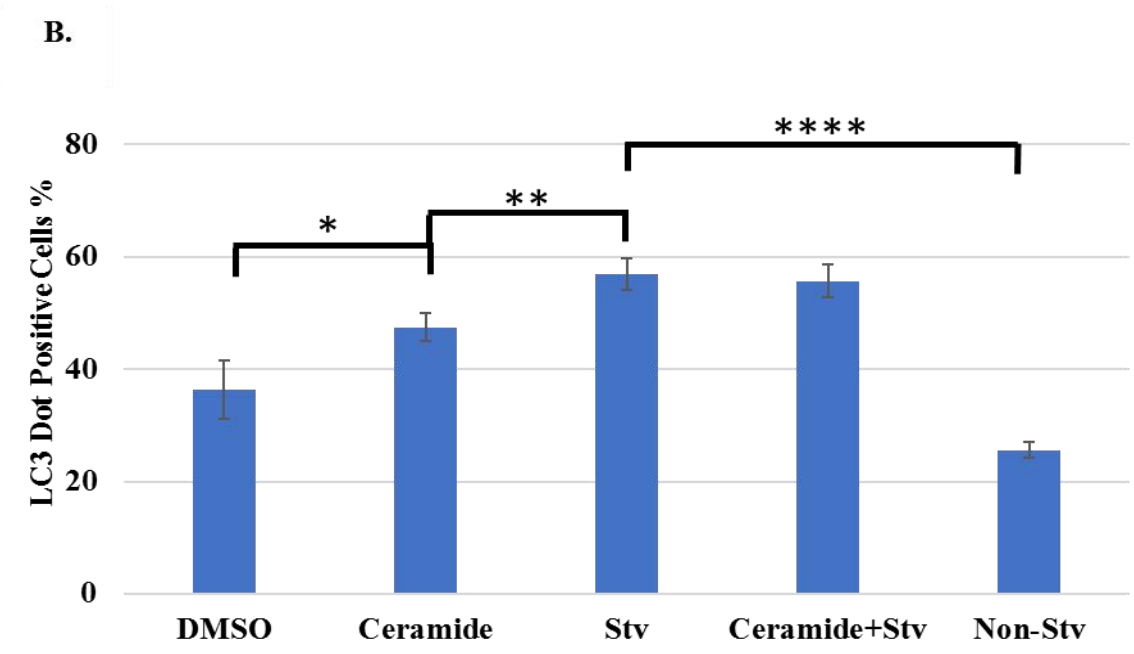

Figure 5.2. GFP-LC3 dot formation upon Ceramide and starvation treatment. (A.) Cells were treated with DMSO or ceramide (1 μM) for 30 minutes and EBSS for 2 hours. Microscopic images were visualized under fluorescence microscopy with 60x objective (B.) Quantification of GFP-LC3 positive cells. Percentage of positive cells in total counted cells (minimum 100 cells) were compared in the graph. DMSO was used as a vehicle control of ceramide. Data were shown as mean ± SD of independent experiments, n=3. *p<0.05, **p<0.01, ***p<0.001, ****p<0.0001.

5.3. Lentivirus Transduction to MEF GFP-LC3 transgenic cells

In the previous part, the alterations in autophagy mechanism were demonstrated under PMA, ceramide and starvation-treated conditions. In order to investigate the relationship of PKC isozymes and their targets in the signaling pathways related to autophagy mechanism, shRNA lentiviral pool infection was performed in MEF GFP-LC3 transgenic cells. shRNA lentiviral pool is a pathway target specific lentivirus mixture containing more than 27000 vectors targeting 4625 genes. Our first aim was to produce lentiviral vectors in HEK293T cells and followed by infection of MEF GFP-LC3 transgenic cells with produced lentivirus pool. Since the final goal was to identify specific targets related with PKC isozymes and their effect on autophagy mechanism, monoclonal cells were generated.

HEK293T cells were transduced with shRNA lentiviral library with calcium phosphate transfection protocol. RFP shRNA control lentiviral vector was used as an empty control. Both helper and envelope plasmids were used in combination with shRNA lentivirus to increase efficiency of virus production in the cells. The ratio of vectors was 5 lentivirus pool; 1 envelop vector pmD2.G; 4 helper vector psPAX2. After transduction of HEK293T cells, the virus titers were collected at 36 and 48 hours. After filteration, MEF GFP-LC3 transgenic cells were transduced with 0, 50, 100, 250 and 500 μl of shRNA lentiviral library or RFP shRNA control vector. 50 μl lentivirus group has lower RFP signals so their propagation might be difficult under antibiotic selection. On the other hand, almost each cell in 250 and 500 μl lentivirus groups have RFP signal so it was suspected that the

cells might have more than one lentivirus infection. We aimed to give one vector to each cell so 250 and 500 µl lentivirus groups were eliminated. The RFP signal ratio in 100 µl lentivirus group was moderate compared to others so we choose to continue antibiotic selection by using this titration (Figure 5.3).

Transduced cells including puromycin resistance gene were subjected to puromycin treatment for 10 days in order to produce monoclonal cells. The cells without lentiviral vectors died in 2 days while propagation of transduced cells increased.

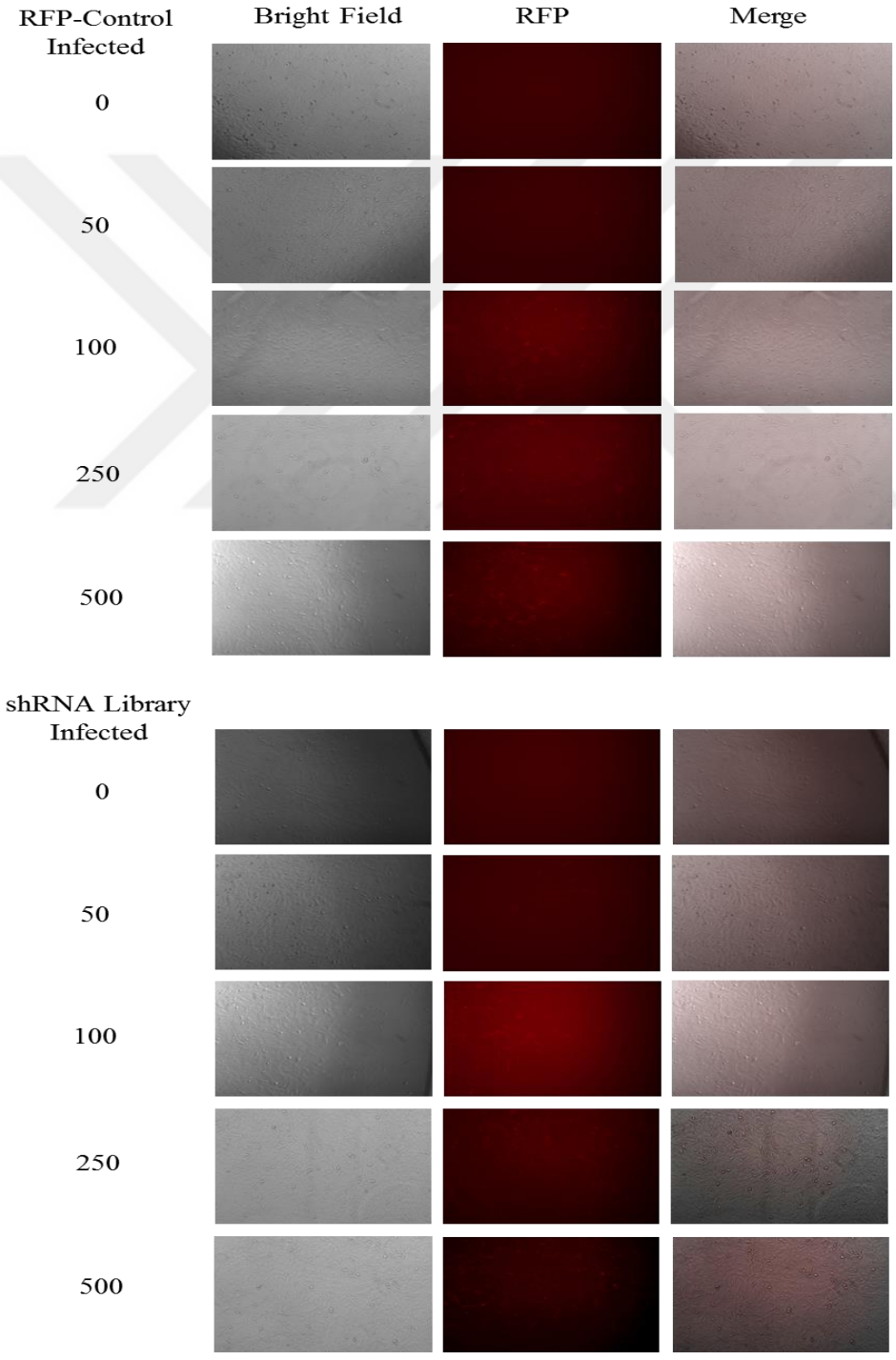

Figure 5.3. Transduction efficiency with different virus titers.

5.4. The effect of PMA and Ceramide treatment on monoclones

After puromycin selection, transduced cells were diluted and seeded in 96 well culture plate. Each well was checked under fluorescence microscopy with green and red channels. The wells including single cell were determined and labelled to follow the further colony growth. 12 monoclones including shRNA lentiviral library and 10 monoclones including RFP shRNA control vector were labelled in 96 well plates, however, half of them died during propagation processes. When each single colony covered 80% of wells, they were transferred to 24 well plate, 12 well plate, 6 well plate and 10 cm culture plate respectively. After growing in 10 cm plate, they were divided into two as one for propagation in order to use for further analysis; one for barcode sequence analysis. Total 6 monoclones having shRNA lentiviral library vector and 3 monoclones having RFP shRNA control vector were produced.

To determine the change in autophagy mechanism after PMA and ceramide treatment, GFP-LC3 puncta count was performed by using each monoclones. It was interesting that autophagic activity was upregulated in some monoclones upon PMA treatment. As indicated in the first section, PMA had inhibitory effect on autophagy in MEF GFP-LC3 transgenic cells. Reverse result of PMA treatment in single cell monoclones supports our hypothesis, that downregulation of specific gene by shRNA causes change in autophagy activation. Especially, MC3 monoclone showed significant increase in autophagy under PMA treatment compared to basal condition (Figure 5.4 A). The downregulation of specific gene in MC3 clone may cause the impairment of autophagy under PKC activation.

Although ceramide treatment induced autophagy in MEF GFP-LC3 transgenic cells indicated as control in Figure 5.4, MC6 single cell monoclone suppressed autophagy upon ceramide treatment in both basal and starvation-induced condition (Figure 5.4 B). This result showed that the decrease in LC3 puncta formation may be due to inhibition of target gene in MC6 monoclone by shRNA.

As expected, starvation condition caused the significant increase in the number of LC3 dots in monoclones. GFP-LC3 dot formation in monoclones was shown in Figure 5.5.

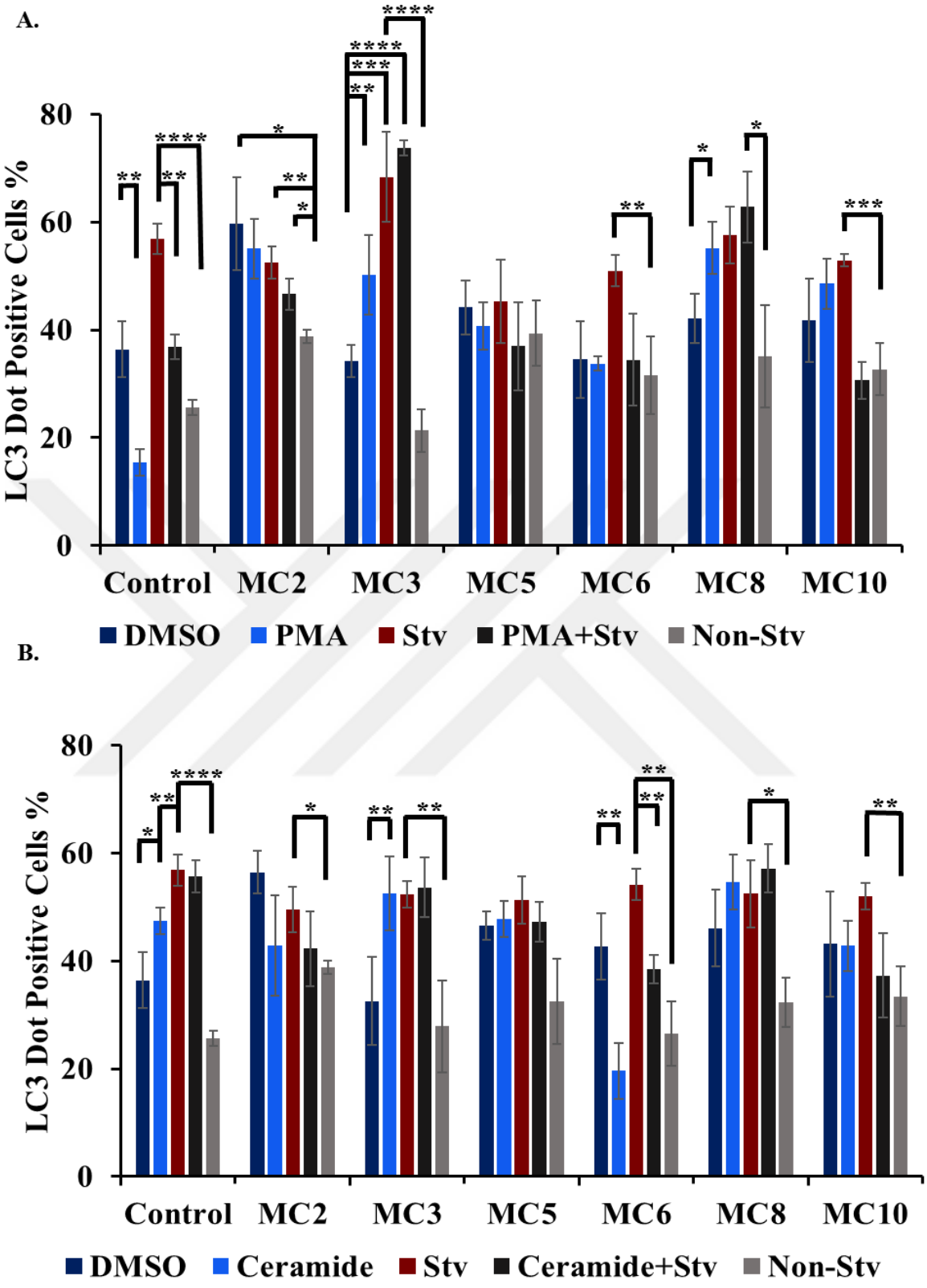

Figure 5.4. GFP-LC3 puncta count upon (A.) PMA and (B.) ceramide treatment in monoclones. DMSO was used as a vehicle control of PMA and ceramide. Control group was results of non-transfected MEF GFP-LC3 cells. Data were shown as mean ± SD of independent experiments, n=3. *p<0.05, **p<0.01, ***p<0.001, ****p<0.0001.

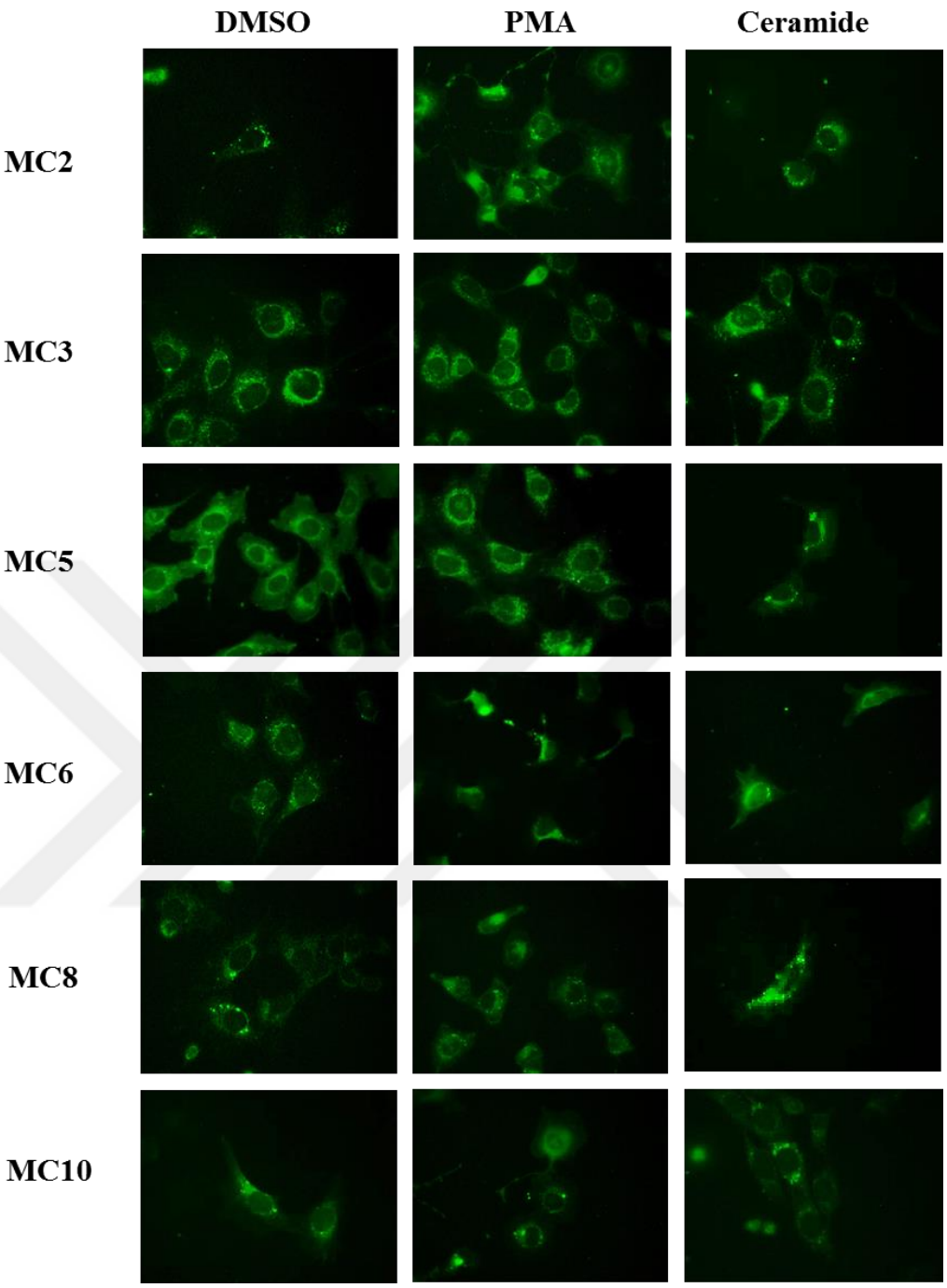

Figure 5.5. GFP-LC3 puncta images upon PMA and ceramide treatment of single cell monoclones under fluorescence microscopy with 60x objective. DMSO was used as a vehicle control of PMA and ceramide.

5.5. Monoclones's Sequence Result

Six different single clones were propagated and their barcode sequence in genomic DNA were amplified with PCR. Four different primer pairs were used in order to amplify barcode sequence or barcode with shRNA sequence. Barcode sequence amplification was represented at Figure 5.6 part A.

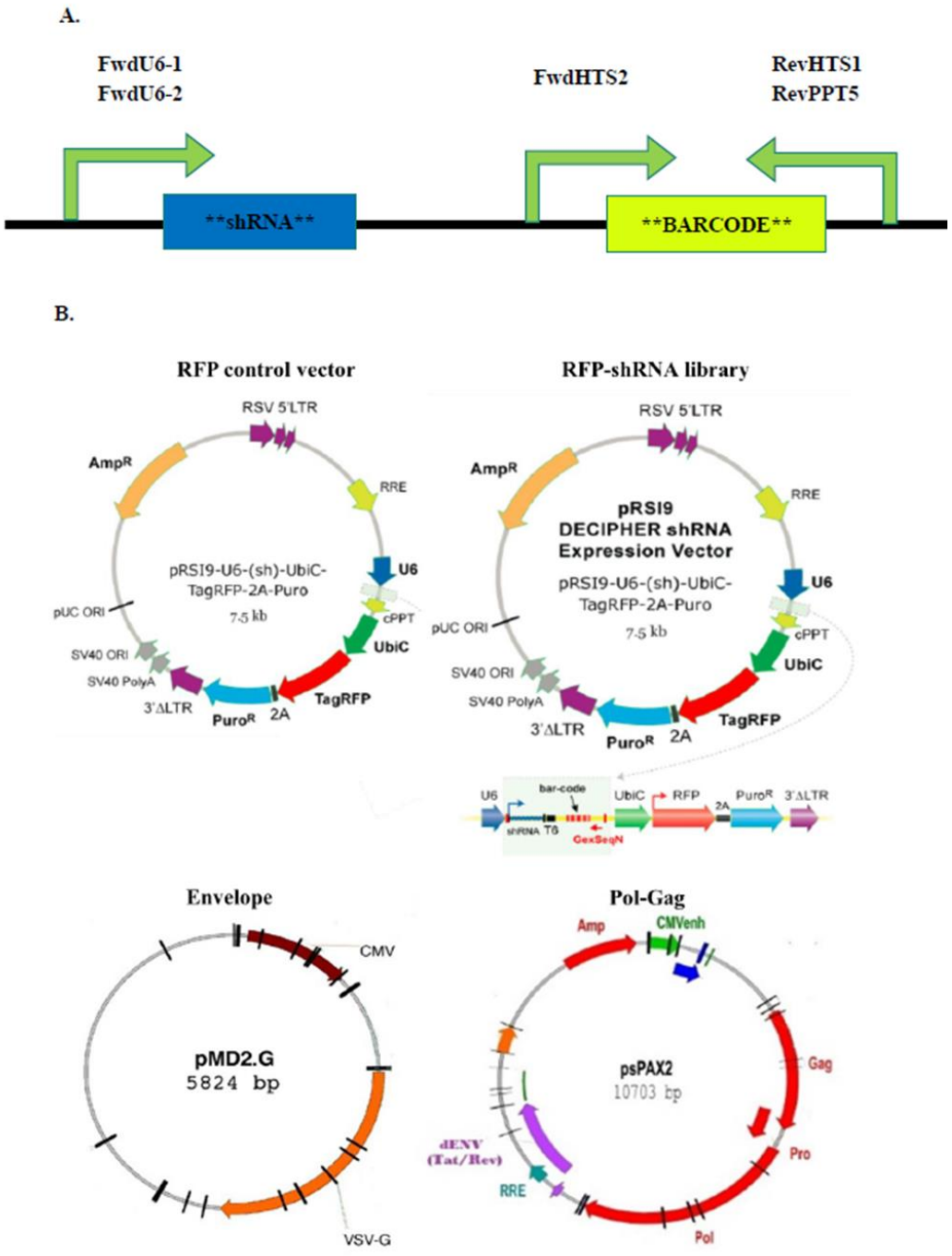

Figure 5.6. Barcode sequence amplification (A.) Representation of primer, barcode and shRNA sites of vector. (B.) Maps of lentivirus plasmids.

PCR products were visualized on agarose gel in order to check the fragment of interest. Forward U61-Reverse PPT5 primer pairs and Forward U62-Reverse PPT5 primer pair amplified both shRNA and barcode sequence together. However, it was observed that this primer pairs also amplified non-specific sequences in genomic DNA of monoclones including RFP shRNA control vector (RC) (Figure 5.7 A-B). The primer pairs were not appropriate for barcode amplification because they were not site specific for shRNA and barcode regions. Forward HTS2-Reverse HTS1 and Forward HTS2-Reverse PPT5 primer pairs were used for only barcode sequence amplification. However, as previous primer pairs, non-specific sequences in genomic DNA of monoclones including RFP shRNA control vector were amplified with Forward HTS2-Reverse HTS1 primer pair (Figure 5.7 C). Meaning that, the primer pair was not specific for barcode sequence amplification. Forward HTS2-Reverse PPT5 primer pair amplified only barcode sequence in monoclones having shRNA and they did not amplify any region in genomic DNA of monoclones including RFP shRNA control vector (Figure 5.7 D).

Agarose gel images showed that only PCR reaction with Forward HTS2 and Reverse PPT5 primer pair gave the correct fragments in monoclones including lentivirus library, but not monoclones including RFP shRNA control vector. PCR products were purified from agarose gel and sent to sequence analysis in order to determine corresponding gene of interest.

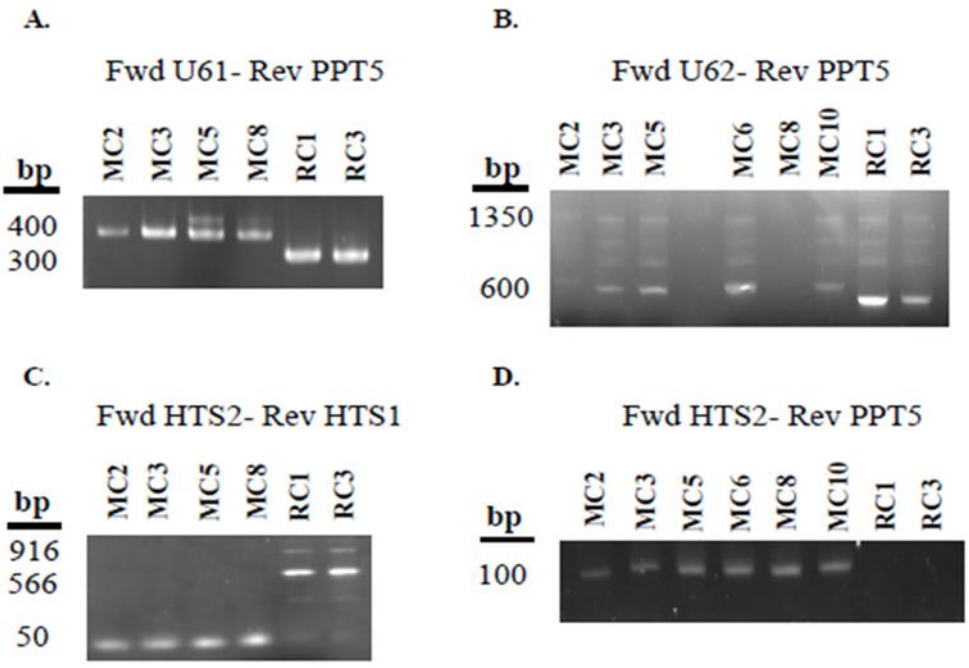

Figure 5.7. Agarose gel images of PCR amplification in monoclones. (A.) PCR product of monoclones amplified with Forward U61-Reverse PPT5 primer pairs. (B.) Forward U62-Reverse PPT5 primer pair. (C.) Forward HTS2-Reverse HTS1 primer pair. (D.) Forward HTS2-Reverse PPT5 primer pair. RC clones were used as negative control, which include only RFP shRNA control vector and did not contain any barcode sequence.

According to the DNA sequence data (Figure 5.8), MC3 monoclone has barcode sequence specific for TRPV6 gene and MC10 monoclone has barcode sequence specific for Rab 23 gene (Table 5.1.).

Cellecta DECIPHER shRNA Library
Mouse Module 1
Signaling Pathway Targets
4,625 Targets, 27,500 shRNA
Cat.# DMPAC-M1-P
shRNA and barcode Sequences
Module Identifier: AT (AT in HT sequencing)
v1a, 2/14/14
(for pRSI9 and pRSI12)
HT Sequencing QC in pRSI12: 3/5/12

CELLECTA

PLEASE NOTE: The DECIPHER shRNA are designed for target mRNA associated with the **RefSeq#**, not the HUGO gene symbol. We can't guarantee that the gene symbols indicated below are accurate, as there may be synonyms, nomenclature updates/changes, or other discrepancies in naming that are beyond our control. Please see the HUGO Gene Nomenclature Committee website at http://www.genenames.org/hgnc-guidelines for more

gene#	gi	RefSeq	HUGO Gene Symbol	CDS/ UTR	sense	sense + mismatches	18-nt barcode	barcode ID
4096	142376464	NM_008143.3	Gnb2l1	CDS	GCAAGATCATTGTAGATGAAT	GCAAGATCATTGTAGATGAAT	TGGTGTCAGTGTTGGTCA	1073
4096	142376464	NM_008143.3	Gnb2l1	CDS	CCGAGACAAGACCATAAAGTT	CCGAGACAAGACtATAAAGTT	CAGTGTCAGTGTTGGTAC	1074
4096	142376464	NM_008143.3	Gnb2l1	CDS	GATGTTGTTATCTCCTCTGAT	GATGTTGTTATCTCCTcTGAT	GTGTGTCAGTGTTGGTTG	1075
4096	142376464	NM_008143.3	Gnb2l1	CDS	TCTGGCTAACTGCAAGCTAAA	TCTGGCTAACTGCAAGcTAAA	TGGTGTCAGTGTTGCAGT	1076
4080	142374373	NM_022413.3	Trpv6	CDS	CCCTACTGGAACTTATTGTTA	CCCTACTGGAAcTTATTGTTA	CAGTACGTCAACACGTAC	8610
2339	86262150	NM_009706.2	Arhgap5	CDS	CCCACAAAGTAAAGGAAGATA	CCCAcAAAGTAAAGGAAGATA	ACGTGTCAGTGTTGCAAC	1078
2339	86262150	NM_009706.2	Arhgap5	CDS	CCCTATAACAACTACCCTGAT	CCCTATAACAACTACCcTGAT	CAGTGTCAGTGTTGCATG	1079
4098	142377153	NM_008999.3	Rab23	CDS	ACACTCAAGTAGTAACAAGAT	ACACTCAAGTAGTAACAAGAT	CAGTTGACTGGTACTGAC	15150
1507	32813438	NM_177262.3	Pknl	CDS	GCACATTCATAGCGACGTGTT	GCACATTcATAGCGAcGTGTT	CAGTGTCAGTGTTGACCA	1081
1507	32813438	NM_177262.3	Pknl	CDS	GCCAGACAGATGAACATAGAT	GCCAGACAGATGAAcATAGAT	TGGTGTCAGTGTTGACAC	1082
1507	32813438	NM_177262.3	Pknl	CDS	GCAGGACAGTAAGACCAAGAT	GCAGGAcAGTAAGACcAAGAT	ACGTGTCAGTGTTGACTG	1083
1507	32813438	NM_177262.3	Pknl	CDS	GCCATCAAAGCCTTGAAGAAA	GCCATCAAAGCcTTGAAGAAA	CAGTGTCAGTGTTGTGGT	1084
2942	142261805	NM_178654.3	Pkn2	CDS	CGGGAAGATGTTAGTAACTTT	CGGGAAGaTGTTAGTAaCTTT	ACGTGTCAGTGTTGTGCA	1085

Figure 5.8. Barcode Sites of monoclones was highlighted at Cellecta shRNA Library document

Table5.1. Sequence Result

Monoclone	NM code	Hugo gene symbol	18-nt- Barcode
MC 10	NM_008999.3	Rab23	CAGTTGACTGGTACTGAC
MC 3	NM_022413.3	Trpv6	CAGTACGTCAACACGTAC

5.6 TRPV6 gene expression and protein level were examined in MC3 monoclone

In order to confirm gene silencing, mRNA expression of TRPV6 under PMA and starvation treatments in MEF GFP-LC3 transgenic cells and MC3 monoclone was examined by RT-q- PCR analysis. Under basal condition mRNA level of TRPV6 in MC3 is significantly lower than MEF GFP-LC3 cells (Figure 5.9 A).

p62 is a receptor for ubiquitinated proteins and directed them to the autophagic degradation. p62 is degraded by autophagy so the decrease in p62 indicates autophagic activity. Increased level of autophagosome-associated LC3 I and increased level of p62 in MEF GFP-LC3 transgenic cells confirmed inhibitory effect of PMA on autophagy (Figure 5.9 B)

While mRNA level of target protein was significantly lower, there was not prominent change in the target protein level in MEF GFP-LC3 transgenic and MC3 monoclones (Figure 5.9 B-C). Under PMA treatment PKCδ expression increased in both basal and starvation-induced condition in MEF GFP-LC3 transgenic and MC3 monoclones (Figure 5.9 B-C). These results indicated that downregulation of TRPV6 gene could be a target of PKCδ that regulate autophagy.

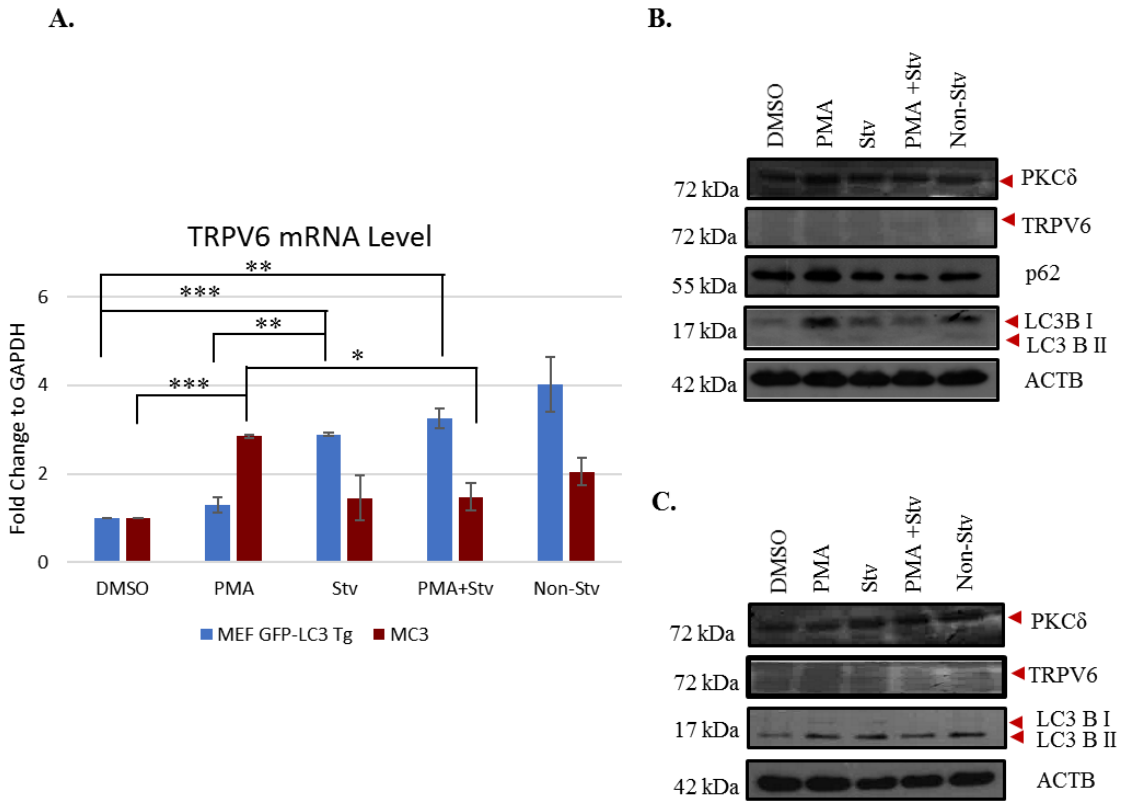

Figure 5.9. Confirmation of gene silencing of TRPV6 and its effect on autophagy in MEF GFP-LC3 transgenic cells (A and B) and MC3 monoclone (A and C) under PMA and starvation-induced conditions. (B and C) Immunoblots showing protein expression of PKCδ, TRPV6, p62 and LC3. Cells were treated with DMSO or PMA (100nM) for 30 minutes and EBSS for 2 hours. ACTB was used as a loading control. Data were shown as mean ± SD of independent experiments, n=3, *p<0.05, **p<0.01, ***p<0.001, ****p<0.0001.

5.7 RAB23 gene expression and protein level were examined in single cell clone

RAB23 gene was the silenced gene according to barcode sequence analysis in MC10. However, mRNA expression of RAB23 in MC10 was not lower than MEF GFP-LC3 cells (Figure 5.10 A). Maybe the sequence result or primer pairs in RT-q-PCR were not completely specific for RAB23. However, it is interesting that under PMA treatment, p62 level was decreased compared to non-starvation and starvation conditions in MC10 cells (Figure 5.10 C.).

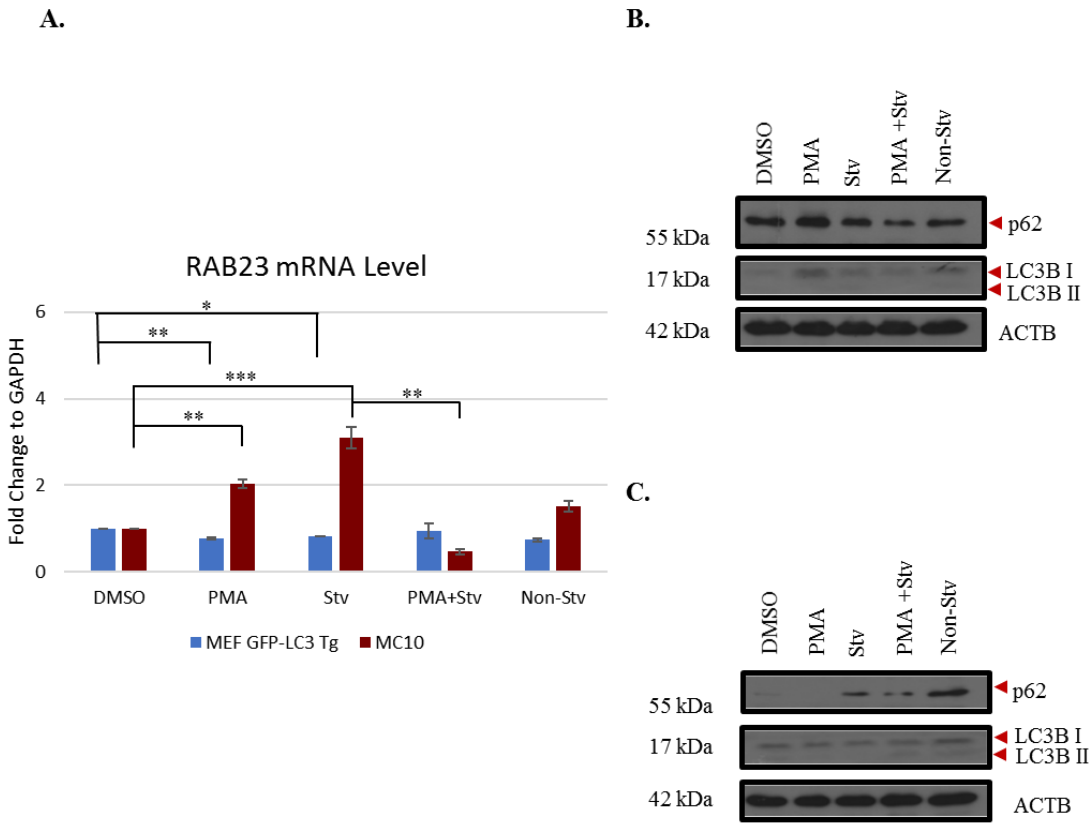

Figure 5.10. Confirmation of gene silencing of RAB23 and its effect on autophagy in MEF GFP-LC3 transgenic cells (A and B) and MC10 monoclone (A and C) under PMA and starvation-induced conditions. (B and C) Immunoblots showing protein expression of p62 and LC3. Cells were treated with DMSO or PMA (100nM) for 30 minutes and EBSS for 2 hours. ACTB was used as a loading control. Data were shown as mean ± SD of independent experiments, n=3, *p<0.05, **p<0.01, ***p<0.001, ****p<0.0001.

5.8 Confirmation of the effect of PMA and expression of TRPV6 in HeLa GFP-LC3 Stable Cells

In the literature, the alteration of TRPV6 expression was detected in development and progression of prostate cancer, lung cancer, ovarian cancer and breast cancer (Haustrate, Hantute-Ghesquier, Prevarskaya, & Lehen'kyi, 2019; Kaemmerer, Turner, Peters, Roberts-Thomson, & Monteith, 2018; Lutes et al., 2018; Song et al., 2018). In the light of that, the interaction of TRPV6 with PKCδ and its effect on autophagy mechanism was aimed to investigate in HeLa GFP-LC3 stable cell line. However, HeLa GFP-LC3 cells could not be transfected by using conventional calcium phosphate (CaPO4) protocol. Therefore, first, transfection efficiency of several methods was analyzed at 48 h post transfection.

Previously, calcium phosphate (CaPO4) transfection protocol was used for HeLa cell line transfection yet, pH of CaPO4 could not be stabilized. Transfection solutions with different pH groups were tested range from 7.00 to 7.20 and GFP signals were only detected at 7.10 and 7.13 pH value but with very low efficiency.

In the literature, lipid or polymer-based transfection reagents such as Lipofectamine and FuGENE were mostly used for HeLa cell line transfection. Instead of CaPO4 transfection, we decided to check the transfection efficiency of electroporation, Lipofectamine 2000, FuGENE 6 or PEI reagents. The flow cytometry result showed that CaPO4 transfection had the lowest efficiency with 5%, while Amaxa Nucleofector transfection had the most efficient transfection with 96%, Lipofectamine 2000 had relatively good efficiency as 70%, FuGENE 6 only transfected 17 % of cells and PEI transfected 5% of cells (Figure 5.12). The cytotoxicity of transfection was also important because higher transfection

efficiency resulted in the decrease of viability. Although the initial number of cells were equal for each transfection group, most of cells died after Amaxa Nucleofector transfection compared to other groups. The rate of dead cells was the least in PEI and CaPO4 transfection groups however changes in cell shape were observed in CaPO4 transfection groups. The cell death was moderate in Lipofectamine 2000 transfection, so we decided to continue further transfection experiments by using Lipofectamine 2000 reagent.

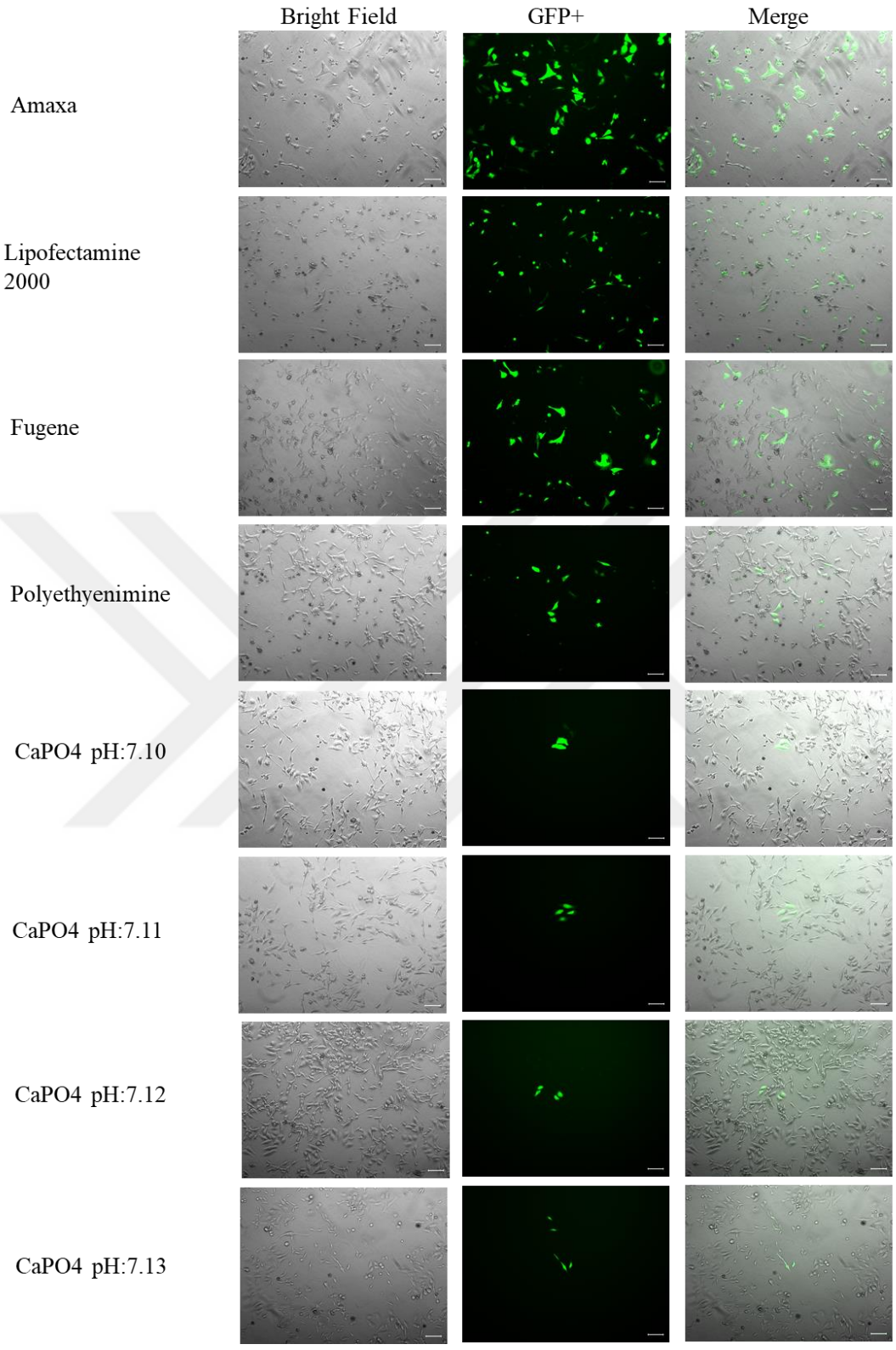

Figure 5.11. Fluorescent microscope images of different transfection methods in HeLa cells at 48 h post transfection.

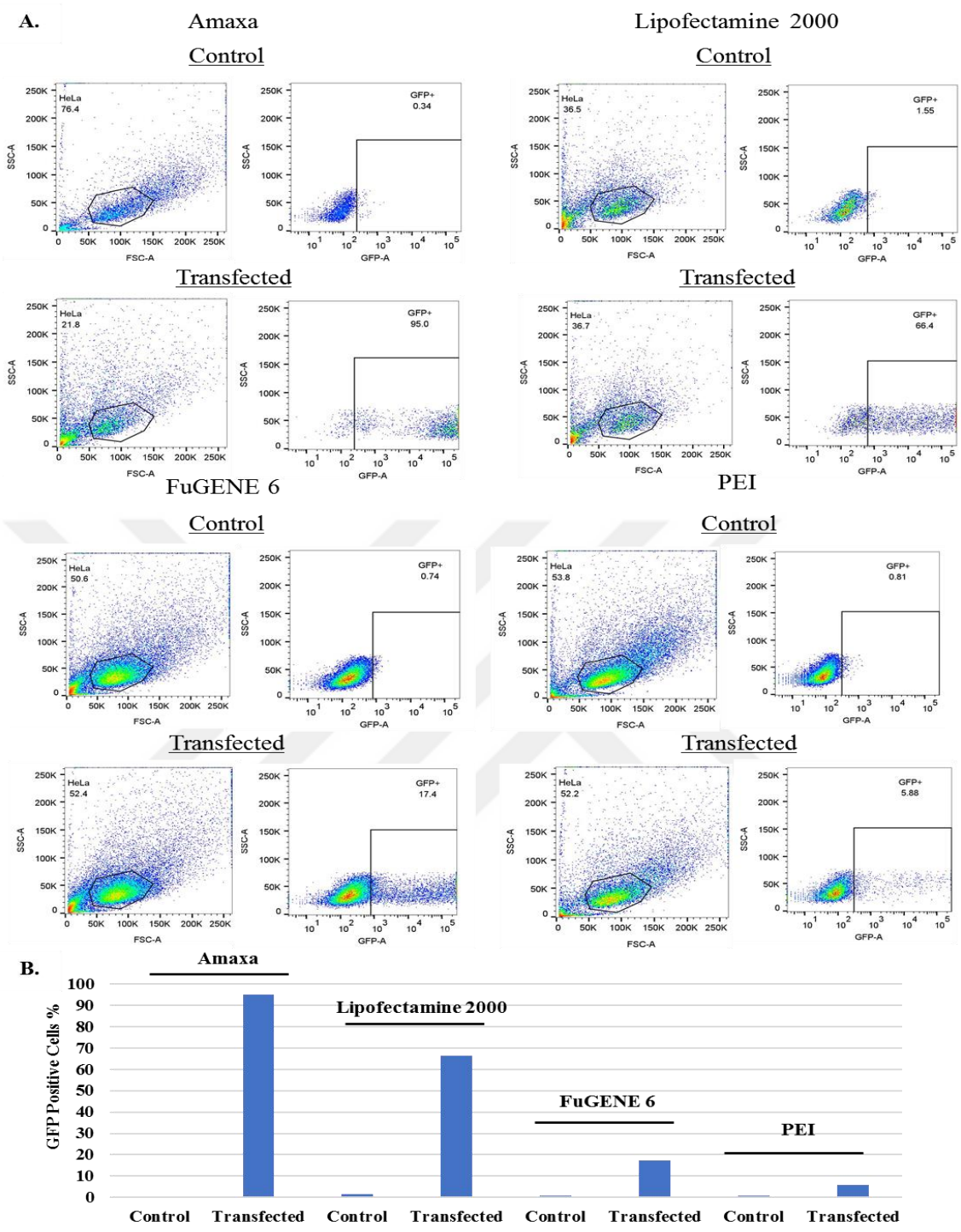
A.
Amaxa
Lipofectamine 2000
Control
Transfected
FuGENE 6
PEI
HeLa
76.4
GFP+
0.34
HeLa
36.5
GFP+
1.55
HeLa
21.8
GFP+
95.0
HeLa
36.7
GFP+
66.4
HeLa
50.6
GFP+
0.74
HeLa
53.8
GFP+
0.81
HeLa
52.4
GFP+
17.4
HeLa
52.2
GFP+
5.88
SSC-A
FSC-A
GFP-A
B.
Amaxa
Lipofectamine 2000
FuGENE 6
PEI
GFP Positive Cells %
100
90
80
70
60
50
40
30
20
10
0
Control
Transfected
Control
Transfected
Control
Transfected
Control
Transfected

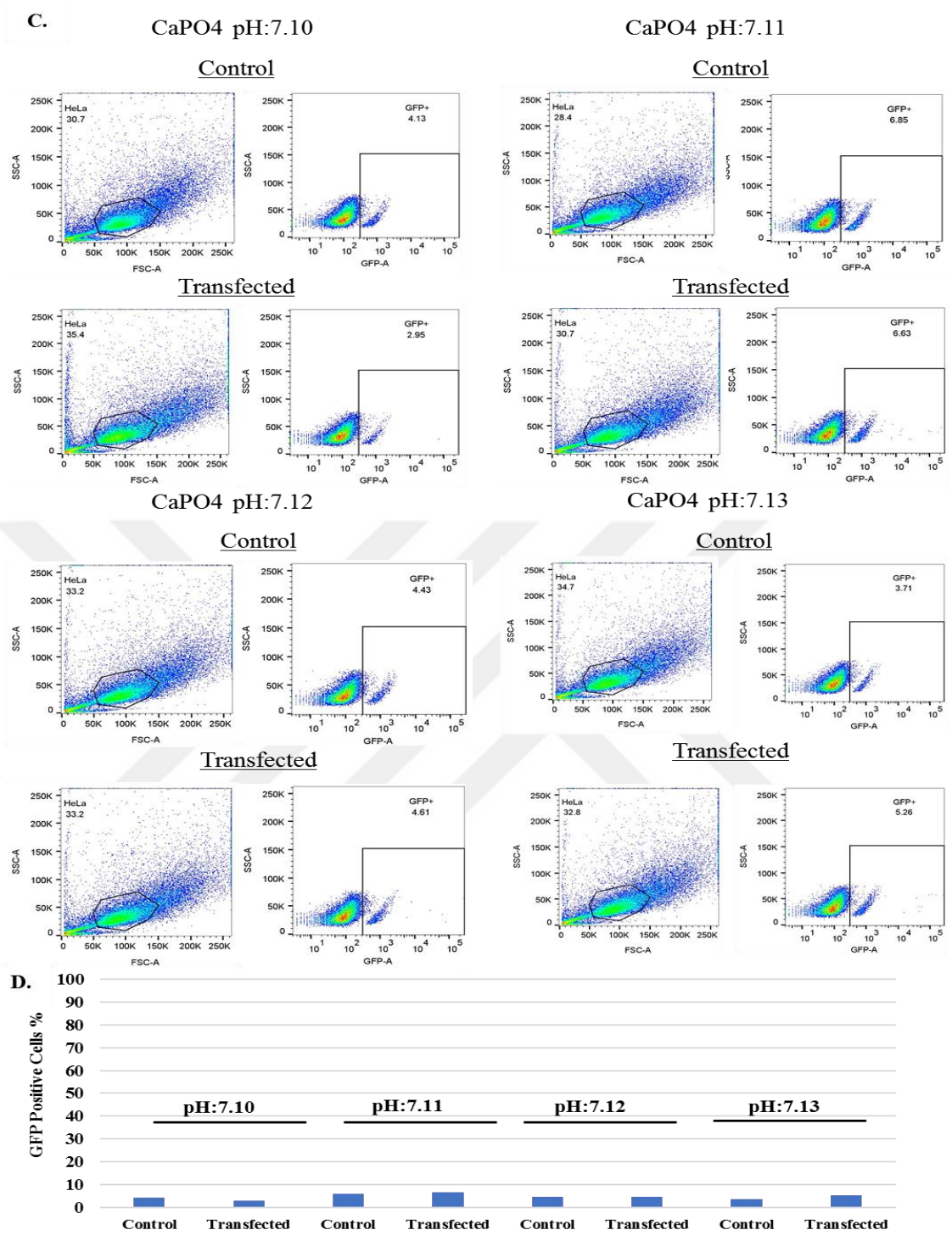

Figure 5.12. Evaluation of the transfection efficiencies of Amaxa Nucleofector, Lipofectamine 2000, FuGENE 6, PEI and CaPO4 protocols in HeLa cells. (A and C) Representative flow cytometry dot plots with percentage of GFP expressing cells. (B and D) Bar chart indicating the percentage of GFP-positive cells in HeLa cells transfected by Amaxa Nucleofector, Lipofectamine 2000, FuGENE 6, PEI and CaPO4. pcDNA3 empty vector was used as control.

Autophagy activity under PMA and starvation conditions was verified with GFP-LC3 dot counting and LC3 II formation (Figure 5.13 A-B) As shown previously, PMA induced PKCδ expression compared to vehicle control DMSO. TRPV6 expression was shown in HeLa GFP-LC3 cells and there was an increase in the TRPV6 expression upon PMA with starvation treatment (Figure 5.13 C).

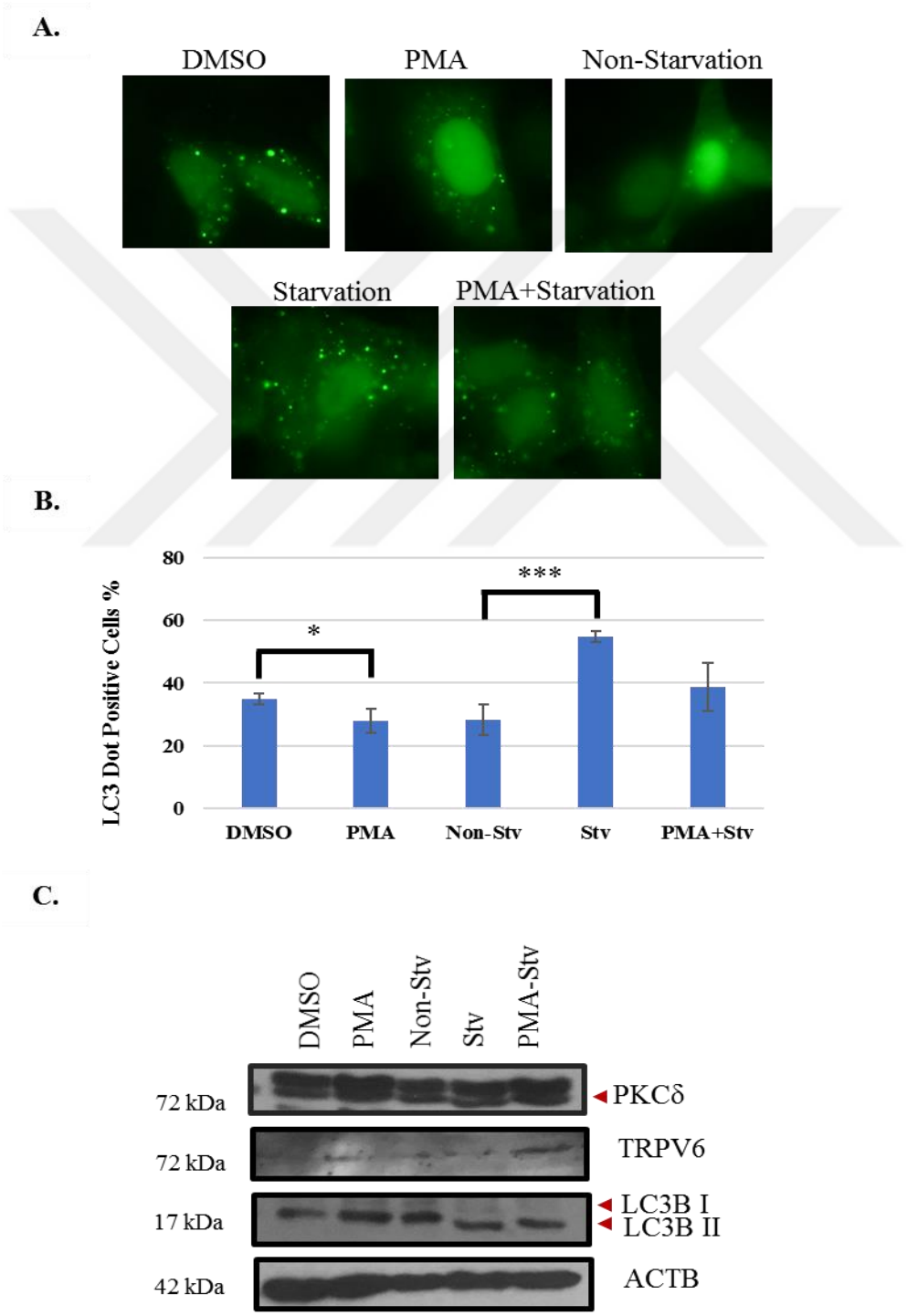

Figure 5.13. The effect of PMA on autophagy in HeLa GFP-LC3 stable cells. (A.) GFP-LC3 dot formation upon PMA and starvation treatment was observed under fluorescence microscopy with 60x objective (B.) Number of GFP-LC3 positive cells in each treatment groups were determined. (C.) Immunoblots showing protein expression of PKCδ, TRPV6 and LC3. Cells were treated with DMSO or PMA (100nM) for 30 minutes and EBSS for 2 hours. ACTB was used as a loading control. Data were shown as mean ± SD of independent experiments, n=3, *p<0.05, **p<0.01, ***p<0.001, ****p<0.0001.

5.9. The effect of overexpression of PKCδ on TRPV6 expression and Autophagy

In order to check the relationship of PKCδ, TRPV6 and autophagy, the effect of PMA and starvation on TRPV6 expression as well as autophagy was investigated by PKCδ overexpression. PKCδ overexpression and PMA treatment caused the increase in the number of LC3 dots (Figure 5.14 A-B). Under PMA treatment, TRPV6 expression was increased compared to control, meanwhile the increase in the degradation of TRPV6 under starvation was reversed with PMA with starvation treatment (Figure 5.14 C).

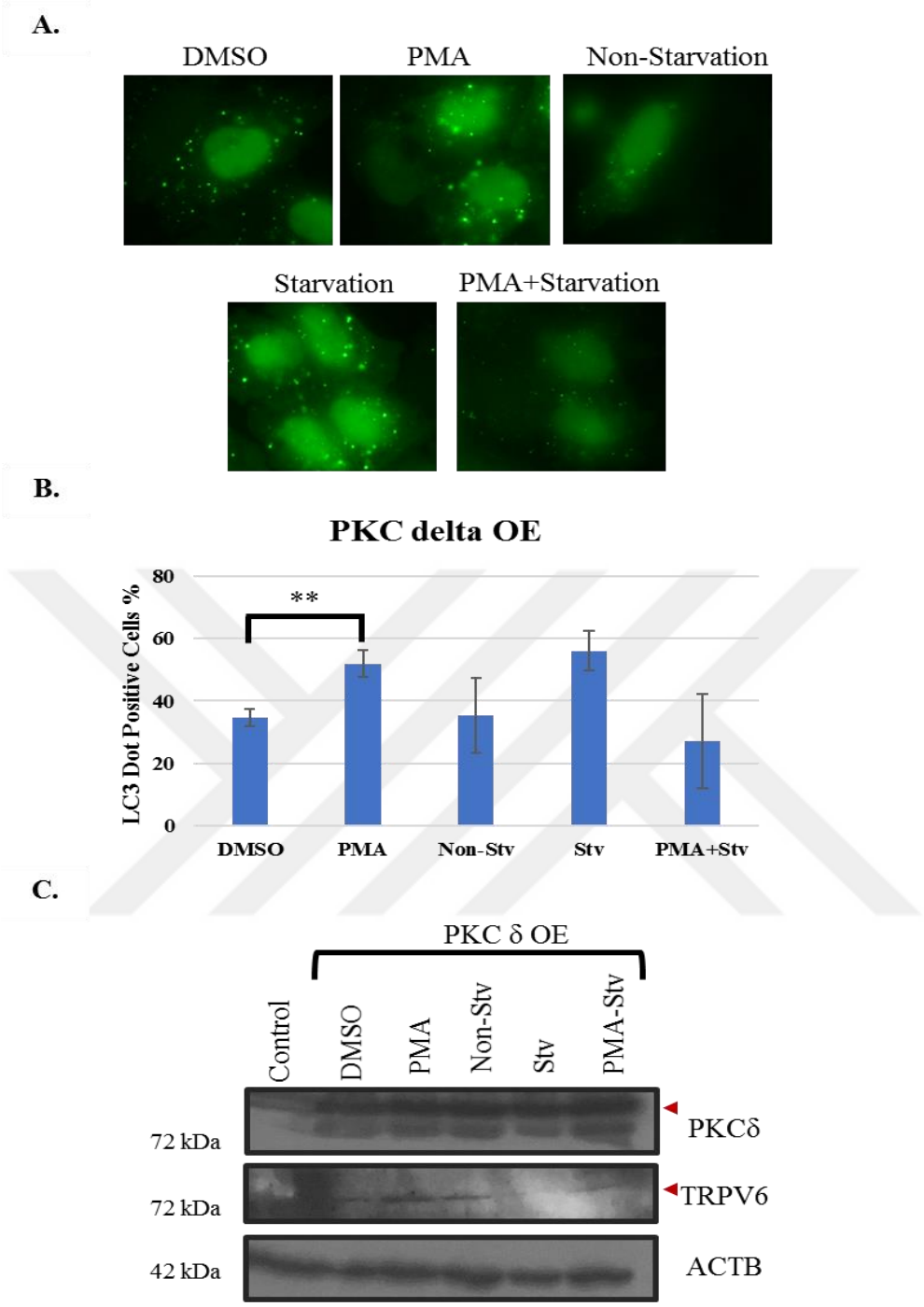

Figure 5.14. The effect of PKCδ overexpression on autophagy in HeLa GFP-LC3 stable cells. (A.) GFP-LC3 dot formation upon PMA and starvation treatment was observed under fluorescence microscopy with 60x objective (B.) Number of GFP-LC3 positive cells in each treatment groups were determined. (C.) Immunoblots showing protein expression of PKCδ, TRPV6 and LC3. Cells were treated with DMSO or PMA (100nM) for 30 minutes and EBSS for 2 hours. ACTB was used as a loading control. Data were shown as mean ± SD of independent experiments, n=3, *p<0.05, **p<0.01, ***p<0.001, ****p<0.0001.

5.10 The effect of PKCδ inhibition on TRPV6 and autophagy

In previous part, it was shown that, the upregulation of PKCδ caused the increase in TRPV6 expression. We wondered whether knockdown of PKCδ by shRNA leads to any alteration in TRPV6 expression. Therefore, PKC delta expression was downregulated by shPKCδ transfection and both autophagy activation and TRPV6 expression were analyzed. While overexpression of PKCδ caused the increase in autophagy activation, shPKCδ knockdown led slight decrease in autophagy (Figure 5.15 A-B). It's remarkable that, the level of TRPV6 was increased with under PKCδ downregulation compared to control and PKCδ overexpression.

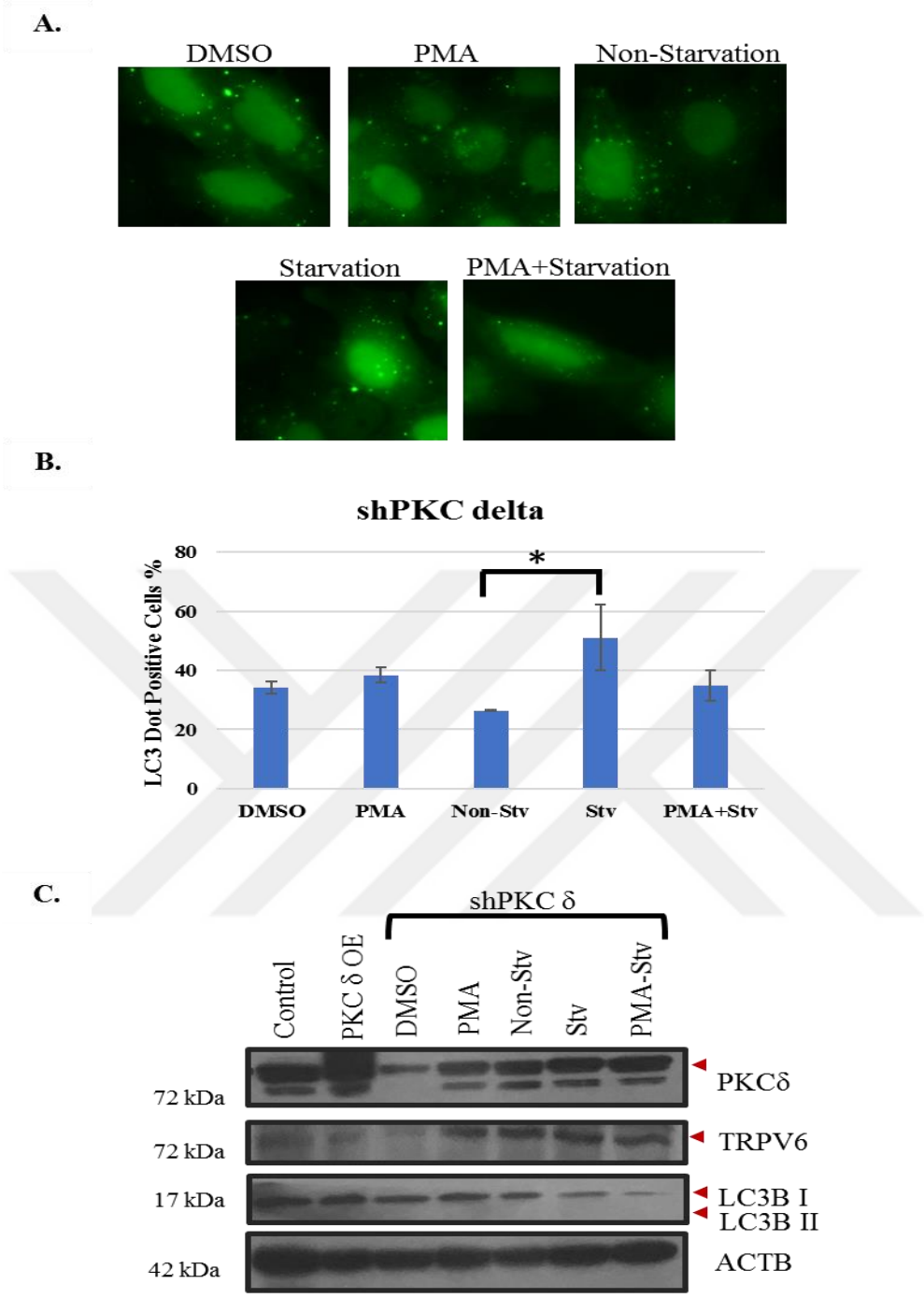

Figure 5.15. The effect of shPKCδ on autophagy and TRPV6 expression in HeLa GFP-LC3 stable cells. (A.) GFP-LC3 dot formation upon PMA and starvation treatment was observed under fluorescence microscopy with 60x objective (B.) Number of GFP-LC3 positive cells in each treatment groups were determined. (C.) Immunoblots showing protein expression of PKCδ, TRPV6 and LC3. Cells were treated with DMSO or PMA (100nM) for 30 minutes and EBSS for 2 hours. ACTB was used as a loading control. Data were shown as mean ± SD of independent experiments, n=3, *p<0.05, **p<0.01, ***p<0.001, ****p<0.0001.

5. 11 Change in PKCδ and autophagy regulation under TRPV6 knockdown

So far, we observed an interaction between TRPV6 and PKCδ and its effect on autophagy mechanism. To understand this interaction, PKCδ expression and autophagy regulation were analyzed under the suppression of TRPV6. It was shown that PKCδ expression could not change upon TRPV6 downregulation (Figure 5. 17 C). As in MC3 monoclone, PMA induced autophagy was observed in TRPV6 suppresed HeLa GFP-LC3 stable cells (Figure 5. 17 A-B). So that downregulation of TRPV6 caused the increase in autophagy activation.

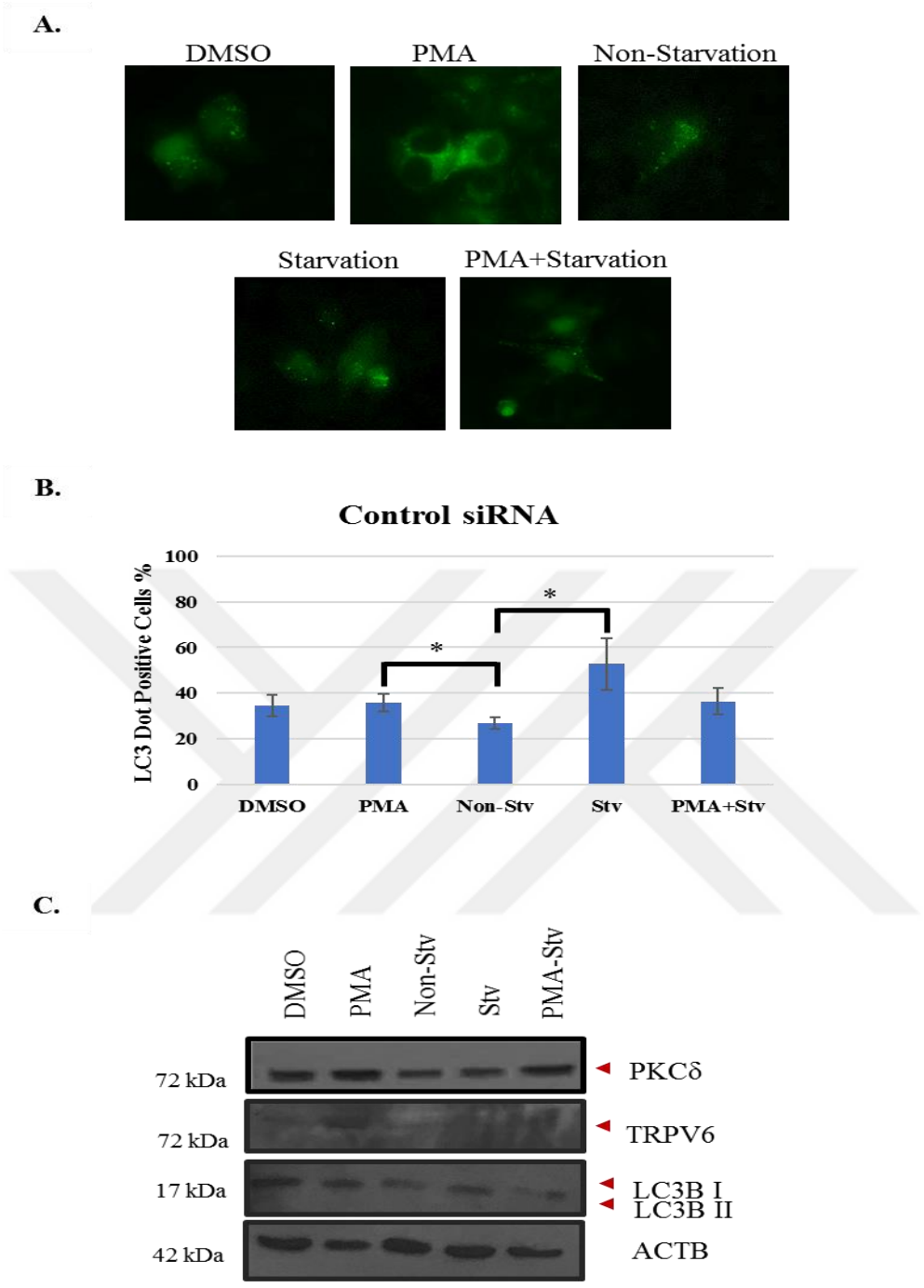

Figure 5.16. The effect of control siRNA on autophagy in HeLa GFP-LC3 stable cells. (A.) GFP-LC3 dot formation upon PMA and starvation treatment was observed under fluorescence microscopy with 60x objective (B.) Number of GFP-LC3 positive cells in each treatment groups were determined. (C.) Immunoblots showing protein expression of PKCδ, TRPV6 and LC3. Cells were treated with DMSO or PMA (100nM) for 30 minutes and EBSS for 2 hours. ACTB was used as a loading control. Data were shown as mean ± SD of independent experiments, n=3, *p<0.05, **p<0.01, ***p<0.001, ****p<0.0001.

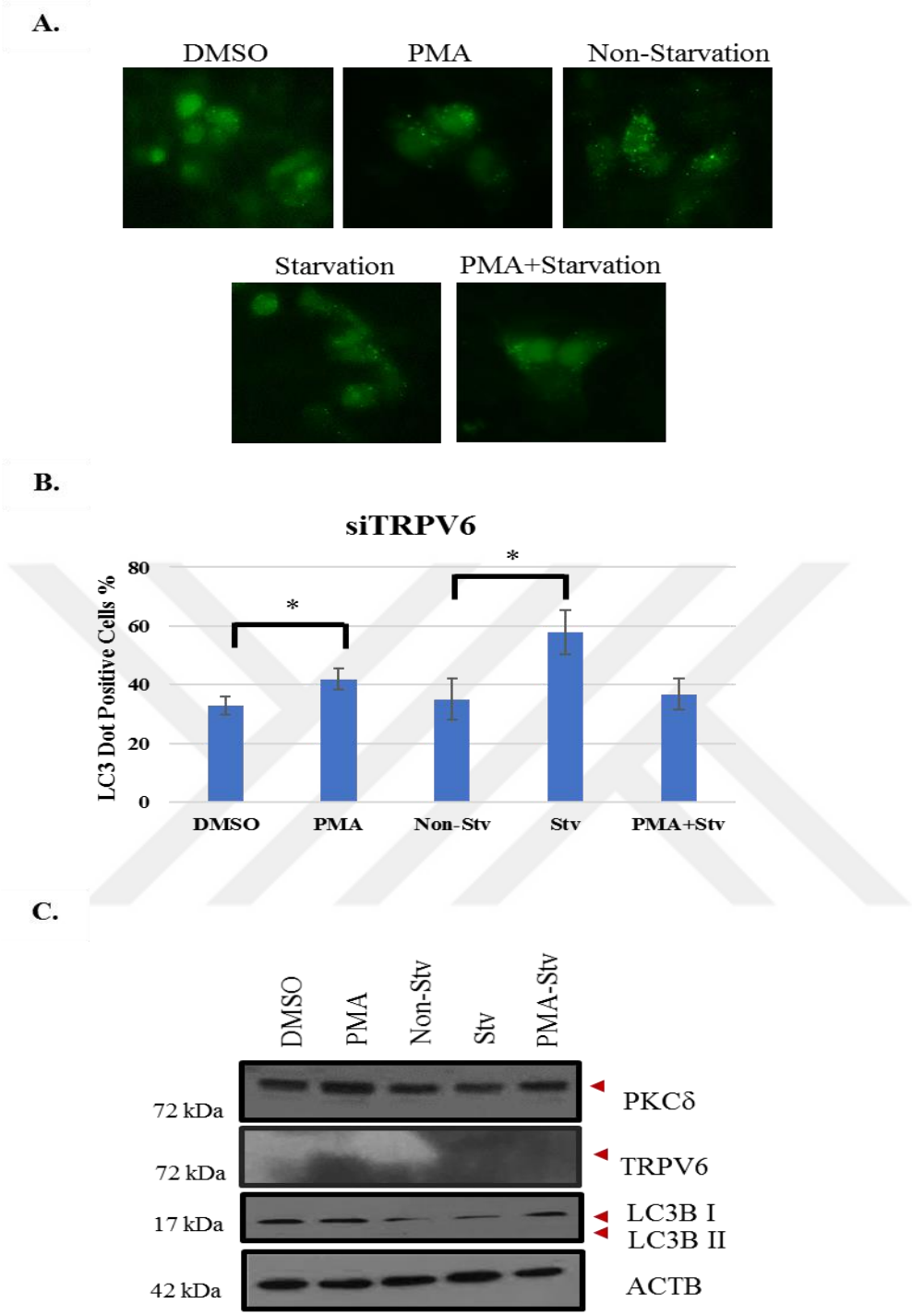

Figure 5.17. The effect of siRPV6 on autophagy in HeLa GFP-LC3 stable cells. (A.) GFP-LC3 dot formation upon PMA and starvation treatment was observed under fluorescence microscopy with 60x objective (B.) Number of GFP-LC3 positive cells in each treatment groups were determined. (C.) Immunoblots showing protein expression of PKCδ, TRPV6 and LC3. Cells were treated with DMSO or PMA (100nM) for 30 minutes and EBSS for 2 hours. ACTB was used as a loading control. Data were shown as mean ± SD of independent experiments, n=3, *p<0.05, **p<0.01, ***p<0.001, ****p<0.0001

5.12 Possible Phosphorylation Sites on TRPV6 and RAB23 by PKCδ

In the literature it was reported that TRPV6 has PKC isozymes mediated phosphorylation sites [86]. In the light of these data, possible phosphorylation sites were predicted by using nine different bioinformatics tools. Accordingly, hit regions that may play a role in the interaction between TRPV6 and PKCδ were shown in Table 5.1. Also, the possible phosphorylation sites on RAB23 by PKCδ were indicated in Table 5.2. Consequently, it was observed that the middle and carboxyl end domains of targets protein may be important for this interaction.

Table 5.2 Predicted Phosphorylation sites of TRPV6 by PKCδ

Residue	GPS 0.5	Phosphomotif	DISPHOS	KinasePhos 2.0	NetPhos 3.1	NetPhorest	PKIS	PhosphoPick	Muside
S-21						*x*	*x*		
S-22	*x*	*x*	*x*				*x*	*x*	*x*
S-44					*x*	*x*	*x*		
S-57	*x*			*x*					
S-68	*x*	*x*	*x*	*x*			*x*	*x*	*x*
S-72							*x*		
S-87							*x*		
T-121				*x*		*x*	*x*		
T-151							*x*		
S-152				*x*		*x*	*x*		
T-159							*x*		
S-182	*x*	*x*	*x*				*x*	*x*	*x*
S-184	*x*	*x*			*x*	*x*	*x*	*x*	
T-188					*x*		*x*	*x*	
S-190					*x*	*x*	*x*	*x*	
S-195	*x*	*x*						*x*	
S-208	*x*			*x*		*x*	*x*	*x*	

S-215				*x*		*x*	*x*		
S-234						*x*	*x*	*x*	
T-238				*x*			*x*		
T-250	*x*						*x*	*x*	
S-261	*x*				*x*	*x*	*x*		
T-282									
T-293									
T-306	*x*	*x*		*x*				*x*	
T-309				*x*	*x*				
T-314						*x*	*x*		
S-315							*x*		
T-316									
T-321									
S-325							*x*		
S-326	*x*								
S-331									
T-337						*x*	*x*		
T-338		*x*			*x*	*x*	*x*	*x*	
T-339	*x*				*x*			*x*	
T-351				*x*				*x*	
S-357						*x*	*x*		
S-358		*x*			*x*				
T-384				*x*					
T-396	*x*	*x*				*x*	*x*	*x*	

T-400									
S-401	*x*	*x*		*x*					*x*
T-406		*x*							
T-419	*x*	*x*							
S-431						*x*	*x*	*x*	
T-452						*x*	*x*	*x*	
T-459				*x*				*x*	
T-471	*x*					*x*			
T-479						*x*		*x*	
S-486	*x*	*x*					*x*	*x*	
S-488				*x*					
S-495						*x*		*x*	
T-519				*x*		*x*			
S-546						*x*		*x*	
T-554				*x*					
S-572							*x*		
T-573	*x*			*x*		*x*			
S-579				*x*					
S-596	*x*			*x*		*x*			
T-598						*x*			
T-607	*x*								
T-621						*x*		*x*	
T-640	*x*			*x*			*x*		
T-641	*x*			*x*				*x*	

S-656									
T-693									
S-696	*x*	*x*			*x*				
S-703		*x*							
S-714				*x*					
S-718	*x*								
S-723			*x*			*x*	*x*		
S-725			*x*						
S-727			*x*		*x*	*x*	*x*	*x*	
T-728	*x*	*x*	*x*		*x*	*x*		*x*	
S-729	*x*	*x*	*x*				*x*		
S-731			*x*				*x*		
S-732	*x*	*x*	*x*			*x*			
T-742	*x*	*x*		*x*	*x*			*x*	*x*
S-760	*x*								

Table 5.3 Predicted Phosphorylation sites of RAB23 by PKCδ

Residue	GPS 0.5	Phosphomotif	DISPHOS	KinasePhos2.0	NetPhos 3.1	Muside
S-24	*x*	*x*			*x*	
S-23						
T-35					*x*	
T-41		*x*				
T-65						
T-75						
S-90				*x*		
T-91						
T-92	*x*	*x*				
S-96	*x*	*x*	*x*			
S-101			*x*			

S-102	*x*	*x*			*x*	
T-116				*x*		
S-129				*x*		
S-150						
S-151	*x*	*x*	*x*		*x*	*x*
T-184						
S-186	*x*			*x*		
S-187						
S-188	*x*	*x*		*x*		
T-196						
S-197						
S-200			*x*			
S-202			*x*			
S-206						
T-208						
T-224	*x*	*x*	*x*	*x*	*x*	*x*
S-232	*x*					
S-233	*x*		*x*			
S-235			*x*			

6. DISCUSSION

Protein kinase C (PKC) isozymes are members of the Serine/Threonine kinase family regulating cellular events through the activation of various signaling pathways. These pathways involve in cell proliferation, development, cellular survival and death mechanisms. It was shown that some PKC isozymes affect autophagy; yet, the exact mechanism of the relationship between PKC isozymes and autophagy is not clearly identified. In this regard, our former group members worked on the identification of PKC isozymes that take place in the autophagy regulation under PKC activators and starvation induced conditions in HeLa cells. Protein level of each PKC isozymes and autophagy activation were examined under PMA, ionomycin and ceramide conditions. According to their data, under PMA treatment which is novel PKC activator, autophagy regulation was suppressed. When they checked the protein level and phosphorylation of PKC isozymes on activation sites, they found specifically increased protein expression and phosphorylation of PKCδ. Also, under ceramide treatment they showed the increase in the autophagy compared to basal condition. Thus, in this thesis, we aimed to identify a novel protein associated with PKC isozymes in the fate of autophagy regulation by shRNA-based gene silencing.

Phosphorylation of LC3 by PKC was found, however the role of phosphorylation on autophagy could not be identified after mutagenesis on phosphorylation sites. This is because the endogenous expression of LC3 was enough to regulate autophagy albeit of mutant LC3 proteins (Jiang, Cheng, Liu, Peng, & Feng, 2010). Also, ULK1 phosphorylation by PKC influenced autophagosome formation negatively because of increasing CMA activity in order to recycle phosphorylated ULK1 proteins (C. Wang et al., 2018). PKCδ activity resulted in the attenuation of autophagy while increasing apoptosis in order to protect kidney cells from cisplatin induced nephrotoxicity. The mechanism occurs due to phosphorylation of AKT and activation of mTOR by PKCδ

(Dongshan Zhang et al., 2017a). Interaction of AKT/mTOR/ULK1 complex with PKC was found important for initiation of autophagy whereas LC3 phosphorylation crucial for autophagosome formation and elongation. Under hypoxic stress, calcium storages in ER were released and caused Ca^{+2} dependent PKCθ activation. PKCθ signaling resulted in the increase in autophagy regulation in hepatic stellate cells (Jin et al., 2016). In another study, critical role of PKCδ in autophagy and apoptosis under hypoxic stress was demonstrated. While under short term stress condition, PKCδ caused the increase in autophagy to protect cells from death, under long term stress PKCδ initiated apoptosis in order to get rid of nonfunctional damaged cells to protect environment (J.-L. Chen et al., 2009; Liu et al., 2019; So & Oh, 2016). Noticeably, PKC signaling has pivotal role in the regulation of autophagy to decide cells' destiny under stress conditions. Thus, investigation of PKC signaling pathways is important to understand the cell death and survival mechanisms in a broader perspective.

In relation to the data, we have previously obtained, in this thesis, it was crucial to show the effect of PKCδ activation on autophagy mechanism in MEF GFP-LC3 transgenic cells upon PMA treatment. PMA showed an inhibitory effect on autophagy consistent with our previous results (Figure 5.1). Ceramide is a specific drug used for the activation of PKCζ. PKCζ is another PKC isozyme that could possibly has function in autophagy regulation, since we showed the change in autophagy activation under ceramide treatment (Figure 5.2).

For further analysis, MEF GFP-LC3 transgenic cells were infected with lentiviral shRNA library, that includes 4625 shRNA targeting genes having role in different signaling pathways. After successful selection with puromycin treatment, monoclonal cells were produced. During monoclone propagation and maintenance, half of them were died. Probably in those monoclones, crucial cell survival genes were silenced so they could not be propagated. Also, the growth rate and cell size were changed after infection in most of monoclones. They grew slower and had smaller surface area compared to non-transduced cells. To determine the change in PMA or ceramide-dependent autophagy, GFP-LC3 puncta count was performed in each monoclones. MC3 monoclone had significant autophagy activation upon PMA treatment under both basal and starvation-induced conditions. This result is significant because PMA had an inhibitory effect on autophagy regulation in non-transduced cells. According to the sequence analysis, the suppressed gene in MC3 monoclone was TRPV6 which is one of the transmembrane calcium

channels. mRNA expression of TRPV6 showed the successful inhibition of target gene by lentiviral shRNA in MC3 monoclone. Previously, PMA treatment showed the inhibition of autophagy in non-transduced MEF GFP-LC3 transgenic cells. However, it was reverse in MC3 monoclone, therefore PMA-induced autophagy might be blocked due to suppression of TRPV6 (Figure 5.9).

TRPV6 is a member of transient receptor potential superfamily and located on both endoplasmic reticulum (ER) and cell membrane. TRPV6 channels are highly sensitive to intracellular Ca^{+2} concentration and acts either homotetrameric or heterotetrameric structure with TRPV5. An increase in Ca^{+2} level results in the inactivation of TRPV6 function via the PLC-PIP2 signaling pathway (Haustrate et al., 2019). The change in expression of TRPV6 was demonstrated in several disease progressions such as carcinogenesis, kidney and cardiac failure due to the disruption of Ca^{+2} uptake (Humeau et al., 2018). Calcium is an essential secondary messenger in signal transduction and has a vital role in cellular homeostasis. Any defect in its turnover may cause blockage of proliferation and initiation of apoptosis since calcium metabolism is important for the cell cycle regulation (Humeau et al., 2018). Excess calcium in the cell is stored in ER and its intracellular signaling initiates from ER to other cellular compartments. Therefore, any fault in intracellular Ca^{+2} balance results in ER stress (Krebs, Agellon, & Michalak, 2015). Recent studies showed that upregulation of TRPV6 protein results in the increase of Ca^{+2} level and causes ER stress mediated apoptosis (J. K. Lau et al., 2014). In contrast, TRPV6 knockdown led to initiation of apoptosis since TRPV6 promotes cell survival by providing apoptosis resistance in cancer (Raphaël et al., 2014). It was reported that ER stress caused by elevated Ca^{+2} level is closely associated with autophagy regulation apart from apoptosis (X. Chen, Li, & Zhao, 2018; Høyer-Hansen & Jäättelä, 2007).

Since the expression of TRPV6 and PKCδ were reported in different type of cancer cells, we decided to perform further experiments in HeLa cell line. In order to apply gene transfer in HeLa cells stably expressing GFP-LC3, we carried out different transfection methods. While, Amaxa transfection demonstrated the highest efficiency, CaPO4 transfection gave the lowest efficiency (Figure 5.11-12). However, the transfection efficiency was proportional to cell death. Therefore, we preferred to use Lipofectamine 2000 which has second efficient transfection results in order to avoid excessive cell death during transfection process. At first, TRPV6 expression and the effect of PMA on autophagy regulation were confirmed in HeLa GFP-LC3 stable cells under basal

condition. In MEF GFP-LC3 transgenic cells, PMA treatment caused an increase in PKCδ protein expression while autophagy was attenuated under this condition. Surprisingly, PMA increased both PKCδ and TRPV6 protein expression compared to both vehicle control and starvation induced condition in HeLa cells (Figure 5.13). It was reported that the change in Ca^{+2} level due to ER stimulation caused autophagy activation however there is not any data regarding to TRPV6 dependent autophagy regulation. Thus, it was important to check the interaction of TRPV6 and PKCδ by establishing overexpression and knockdown experiments.

Our findings demonstrated that upon PMA exposure, autophagy was inhibited due to PKCδ activation. However, PKCδ overexpression caused an increase in the autophagy mechanism upon PMA treatment. This increase might be due to the contrary effect of cellular mechanisms in order to keep cellular homeostasis under excessive amount of PKCδ protein. Meanwhile, in these cells, PMA treatment caused the increase in TRPV6 protein expression in both basal and starvation-induced condition (Figure 5.14). One possibility is that upregulation of PKCδ caused the change in TRPV6 activity and led to Ca^{+2} dependent ER stress and eventually contributed the increase in autophagy under PMA treatment. The another one is that other PKC isozymes activated by PMA may take place in the signaling mechanism and caused the increase in ER stress independent autophagy regardless of TRPV6 activation.

The next step was confirmation of autophagy activity and TRPV6 expression under PKCδ silenced conditions. We expected that under the suppression of PKCδ, TRPV6 protein level could be decreased because both PMA treatment and PKCδ overexpression caused increase in the TRPV6 protein expression. However, it was observed that the expression level of TRPV6 was higher in PKCδ silenced cells under both PMA and starvation induced condition (Figure 5.15). PKCδ downregulation affected TRPV6 expression significantly because TRPV6 could interact with other PKC isozymes in order to stabilize channel activity and to normalize intracellular Ca^{+2} concentration in the absence of enough PKCδ activity. In the literature PKCα dependent phosphorylation of TRPV6 resulted in the change of channel function (Niemeyer, Bergs, Wissenbach, Flockerzi, & Trost, 2001). However, PKCα activation depends on Ca^{+2} so other signaling pathways may ensue to regulate TRPV6 stimulation under PKCδ silenced condition.

These results showed that there is a momentous interaction between PKCδ and TRPV6. The regulation of TRPV6 depends on PKCδ however we wonder whether PKCδ expression relates to the change in TRPV6 expression. In order to examine this hypothesis, we downregulated TRPV6 expression by siRNA silencing to determine both autophagic activity and PKCδ expression. Consistent with MC3 cells, suppression of TRPV6 increased the autophagy upon PMA treatment compared to control in HeLa cells. However, TRPV6 downregulation did not change the PKCδ expression (Figure 5.17). Therefore, the relation between PKCδ and TRPV6 is not mutual. In the literature, TRPV6 works both alone or dual with TRPV5 and they have a similar role in Ca^{+2} regulation. Thus, TRPV5 can substitute TRPV6 role in Ca^{+2} metabolism under the absence of TRPV6.

The change in TRPV6 expression could not cause differences in PKCδ level so we hypothesized that the phosphorylation of TRPV6 by PKCδ may happen. Before experimental process, we aimed to determine possible phosphorylation sites on TRPV6 by PKCδ by using different bioinformatics tools. Interestingly, there were several phosphorylation sites detected and the most common sites located on the N terminus of TRPV6 which is crucial for function of channel activity (Table 5.1, Figure 6.1). Obviously to be determine which sites is important for PKCδ interaction during autophagy regulation, in-depth search should be applied. Our preliminary findings are important because of introducing novel signaling pathway of PKC on autophagy mechanism. Investigation of this pathway will contribute the understanding of PKCδ dependent autophagy activation associated with calcium metabolism clearly.

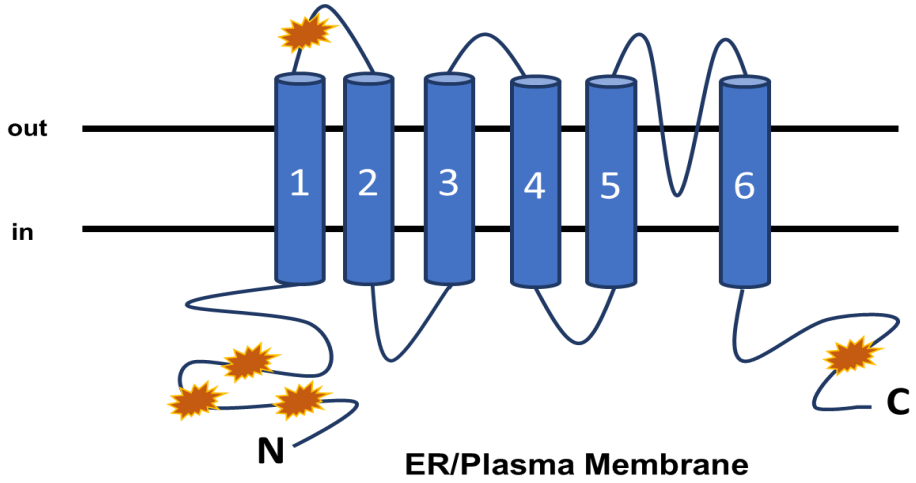

Figure 6.1. Possible phosphorylation sites on TRPV6 targeted by PKCδ were shown in yellow.

7. FUTURE PERSPECTIVE

In this M.Sc. thesis, it was described that PKCδ isozyme interacts with TRPV6, which could have a significant impact on autophagy regulation. The exact mechanism of this interaction could not be identified so far. Our study might be critical, because we investigated possible linker signaling member, TRPV6, to clarify PKCδ mediated autophagy regulation. There are several phosphorylation sites on TRPV6 targeted by PKCδ and point mutations on these sites will lighten the site-specific interaction between TRPV6 and PKCδ. In addition to phosphorylation, the interactions between TRPV6 and PKCδ should be shown by co-immunoprecipitation assays to understand the relation between PKCδ and TRPV6 in terms of binding.

Also, intracellular Ca^{+2} levels should be determined under each treatment condition in order to predict whether these data are related to ER stress-mediated autophagy. Depending on the Ca^{+2} level analysis, Ca^{+2} induced PKCα activation may be checked under both PMA and ionomycin treatment. It is already shown that PKCα can phosphorylate TRPV6. It will clarify whether the change in TRPV6 is depending on PMA or Ca^{+2} concentration. Flow cytometry analysis after FURA-2AM exposure may give idea about cytoplasmic Ca^{+2} concentration related with TRPV6 activity. Also, ER stress inducers such as tunicamycin or thapsigargin may be used as positive control of ER stress during analysis of Ca^{+2} level in cells after PMA and starvation treatments. Also, Ca^{+2} concentration in ER maybe visualized under fluorescence microscopy after FURA 2AM staining and this will contribute the comparison of TRPV6 role in Ca^{+2} concentration both in ER and cytoplasm.

PKC isozymes may have contrary effects on autophagy depending on the cell types. In order to show PKCδ and TRPV6 relation, different cancer cell lines might be used to confirm this interaction on autophagy mechanism.

8. REFERENCES

Alers, S., Löffler, A. S., Wesselborg, S., & Stork, B. (2012). Role of AMPK-mTOR-Ulk1/2 in the regulation of autophagy: cross talk, shortcuts, and feedbacks. *Molecular and cellular biology, 32*(1), 2-11.

Bolsover, S. R., Gomez-Fernandez, J. C., & Corbalan-Garcia, S. (2003). Role of the Ca2+/phosphatidylserine binding region of the C2 domain in the translocation of protein kinase Cα to the plasma membrane. *Journal of Biological Chemistry, 278*(12), 10282-10290.

Chen, J.-L., Lin, H. H., Kim, K.-J., Lin, A., Ou, J.-h. J., & Ann, D. K. (2009). PKCδ signaling: A dual role in regulating hypoxic stress-induced autophagy and apoptosis. *Autophagy, 5*(2), 244-246.

Chen, X., Li, K., & Zhao, G. (2018). Propofol Inhibits HeLa Cells by Impairing Autophagic Flux via AMP-Activated Protein Kinase (AMPK) Activation and Endoplasmic Reticulum Stress Regulated by Calcium. *Medical science monitor : international medical journal of experimental and clinical research, 24*, 2339-2349.

Chen, Y., & Klionsky, D. J. (2011). The regulation of autophagy - unanswered questions. *Journal of cell science, 124*(Pt 2), 161-170.

Crighton, D., Wilkinson, S., O'Prey, J., Syed, N., Smith, P., Harrison, P. R., . . . Ryan, K. M. (2006). DRAM, a p53-Induced Modulator of Autophagy, Is Critical for Apoptosis. *Cell, 126*(1), 121-134.

De Duve, C., Pressman, B. C., Gianetto, R., Wattiaux, R., & Appelmans, F. (1955). Tissue fractionation studies. 6. Intracellular distribution patterns of enzymes in rat-liver tissue. *The Biochemical journal, 60*(4), 604-617.

https://www.ncbi.nlm.nih.gov/pmc/articles/PMC1216159/.

Deas, E., Plun-Favreau, H., Gandhi, S., Desmond, H., Kjaer, S., Loh, S. H. Y., . . . Wood, N. W. (2011). PINK1 cleavage at position A103 by the mitochondrial protease PARL. *Human molecular genetics, 20*(5), 867-879.

Devereaux, K., Dall'Armi, C., Alcazar-Roman, A., Ogasawara, Y., Zhou, X., Wang, F., . . . Di Paolo, G. (2013). Regulation of mammalian autophagy by class II and III PI 3-kinases through PI3P synthesis. *PloS one, 8*(10), e76405.

Edwards, A. S., & Newton, A. C. (1997). Regulation of protein kinase C βII by its C2 domain. *Biochemistry, 36*(50), 15615-15623.

Feng, Z., Zhang, H., Levine, A. J., & Jin, S. (2005). The coordinate regulation of the p53 and mTOR pathways in cells. *Proceedings of the National Academy of Sciences, 102*(23), 8204-8209.

Finn, P. F., & Dice, J. F. (2005). Ketone bodies stimulate chaperone-mediated autophagy. *Journal of Biological Chemistry, 280*(27), 25864-25870.

Glick, D., Barth, S., & Macleod, K. F. (2010). Autophagy: cellular and molecular mechanisms. *The Journal of pathology, 221*(1), 3-12.

Gonnella, R., Granato, M., Farina, A., Santarelli, R., Faggioni, A., & Cirone, M. (2015). PKC theta and p38 MAPK activate the EBV lytic cycle through autophagy induction. *Biochimica et Biophysica Acta (BBA) - Molecular Cell Research, 1853*(7), 1586-1595.

Green, D. R., & Kroemer, G. (2004). The Pathophysiology of Mitochondrial Cell Death. *Science, 305*(5684), 626-629.

Hafeez, B. B., Zhong, W., Weichert, J., Dreckschmidt, N. E., Jamal, M. S., & Verma, A. K. (2011). Genetic ablation of PKC epsilon inhibits prostate cancer development and metastasis in transgenic mouse model of prostate adenocarcinoma. *Cancer research, 71*(6), 2318-2327.

Hanada, T., Noda, N. N., Satomi, Y., Ichimura, Y., Fujioka, Y., Takao, T., . . . Ohsumi, Y. (2007). The Atg12-Atg5 conjugate has a novel E3-like activity for protein lipidation in autophagy. *Journal of Biological Chemistry, 282*(52), 37298-37302.

Haustrate, A., Hantute-Ghesquier, A., Prevarskaya, N., & Lehen'kyi, V. y. (2019). TRPV6 calcium channel regulation, downstream pathways, and therapeutic targeting in cancer. *Cell calcium*.

Høyer-Hansen, M., & Jäättelä, M. (2007). Connecting endoplasmic reticulum stress to autophagy by unfolded protein response and calcium. *Cell Death & Differentiation, 14*(9), 1576-1582.

Hua, R., Han, S., Zhang, N., Dai, Q., Liu, T., & Li, J. (2018). cPKCγ-Modulated Sequential Reactivation of mTOR Inhibited Autophagic Flux in Neurons Exposed to Oxygen Glucose Deprivation/Reperfusion. *International journal of molecular sciences, 19*(5), 1380.

https://www.ncbi.nlm.nih.gov/pmc/articles/PMC5983661/.

Huang, K.-P. (1989). The mechanism of protein kinase C activation. *Trends in Neurosciences, 12*(11), 425-432.

Huang, S.-P., Chien, J.-Y., & Tsai, R.-K. (2015). Ethambutol induces impaired autophagic flux and apoptosis in the rat retina. *Disease models & mechanisms, 8*(8), 977-987.

Humeau, J., Bravo-San Pedro, J. M., Vitale, I., Nuñez, L., Villalobos, C., Kroemer, G., & Senovilla, L. (2018). Calcium signaling and cell cycle: Progression or death. *Cell calcium, 70*, 3-15.

Igumenova, T. I. (2015). Dynamics and membrane interactions of protein kinase C. *Biochemistry*, *54*(32), 4953-4968.

Jha, J. C., Thallas-Bonke, V., Banal, C., Gray, S. P., Chow, B. S. M., Ramm, G., . . . Jandeleit-Dahm, K. A. (2016). Podocyte-specific Nox4 deletion affords renoprotection in a mouse model of diabetic nephropathy. *Diabetologia, 59*(2), 379-389.

Jiang, H., Cheng, D., Liu, W., Peng, J., & Feng, J. (2010). Protein kinase C inhibits autophagy and phosphorylates LC3. *Biochemical and Biophysical Research Communications, 395*(4), 471-476.

Jin, Y., Bai, Y., Ni, H., Qiang, L., Ye, L., Shan, Y., & Zhou, M. (2016). Activation of autophagy through calcium-dependent AMPK/mTOR and PKCθ pathway causes activation of rat hepatic stellate cells under hypoxic stress. *FEBS Letters, 590*(5), 672-682.

Johnson, J. E., Giorgione, J., & Newton, A. C. (2000). The C1 and C2 domains of protein kinase C are independent membrane targeting modules, with specificity for phosphatidylserine conferred by the C1 domain. *Biochemistry, 39*(37), 11360-11369.

Jung, C. H., Ro, S.-H., Cao, J., Otto, N. M., & Kim, D.-H. (2010). mTOR regulation of autophagy. *FEBS letters, 584*(7), 1287-1295.

Kaemmerer, E., Turner, D., Peters, A. A., Roberts-Thomson, S. J., & Monteith, G. R. (2018). An automated epifluorescence microscopy imaging assay for the identification of phospho-AKT level modulators in breast cancer cells. *Journal of Pharmacological and Toxicological Methods, 92*, 13-19.

Kaushik, S., & Cuervo, A. M. (2018). The coming of age of chaperone-mediated autophagy. *Nature reviews. Molecular cell biology, 19*(6), 365-381.

Krebs, J., Agellon, L. B., & Michalak, M. (2015). Ca2+ homeostasis and endoplasmic reticulum (ER) stress: An integrated view of calcium signaling. *Biochemical and Biophysical Research Communications, 460*(1), 114-121.

Lau, J. K., Brown, K. C., Dom, A. M., Witte, T. R., Thornhill, B. A., Crabtree, C. M., . . . Dasgupta, P. (2014). Capsaicin induces apoptosis in human small cell lung cancer via the TRPV6 receptor and the calpain pathway. *Apoptosis, 19*(8), 1190-1201.

Lau, W. M., Teng, E., Huang, K. K., Tan, J. W., Das, K., Zang, Z., . . . So, J. B. Y. (2018). Acquired Resistance to FGFR Inhibitor in Diffuse-Type Gastric Cancer through an AKT-Independent PKC-Mediated Phosphorylation of GSK3β. *Molecular Cancer Therapeutics, 17*(1), 232-242.

Lazarou, M., Jin, S. M., Kane, L. A., & Youle, R. J. (2012). Role of PINK1 binding to the TOM complex and alternate intracellular membranes in recruitment and activation of the E3 ligase Parkin. *Developmental cell, 22*(2), 320-333.

Lee, D.-F., Kuo, H.-P., Chen, C.-T., Hsu, J.-M., Chou, C.-K., Wei, Y., . . . Huang, W.-C. (2007). IKKβ suppression of TSC1 links inflammation and tumor angiogenesis via the mTOR pathway. *Cell, 130*(3), 440-455.

Leitges, M. (2007). Functional PKC in vivo analysis using deficient mouse models. *Biochemical Society Transactions, 35*(5), 1018.

Levine, B., & Abrams, J. (2008). p53: The Janus of autophagy? *Nature cell biology, 10*(6), 637.

Levine, B., & Klionsky, D. J. (2017). Autophagy wins the 2016 Nobel Prize in Physiology or Medicine: Breakthroughs in baker's yeast fuel advances in biomedical research. *Proceedings of the National Academy of Sciences of the United States of America, 114*(2), 201-205.

https://www.ncbi.nlm.nih.gov/pmc/articles/PMC5240711/.

Levine, B., & Kroemer, G. (2008). Autophagy in the pathogenesis of disease. *Cell, 132*(1), 27-42.

Li, N., & Zhang, W. (2017). Protein kinase C β inhibits autophagy and sensitizes cervical cancer Hela cells to cisplatin. *Bioscience reports, 37*(2), BSR20160445.

https://www.ncbi.nlm.nih.gov/pmc/articles/PMC5469325/.

Li, W.-w., Li, J., & Bao, J.-k. (2012). Microautophagy: lesser-known self-eating. *Cellular and molecular life sciences, 69*(7), 1125-1136.

Liu, S., Shen, M., Li, C., Wei, Y., Meng, X., Li, R., . . . Liu, H. (2019). PKCδ contributes to oxidative stress-induced apoptosis in porcine ovarian granulosa cells via activating JNK. *Theriogenology, 131*, 89-95.

Lutes, T., Davey, M., Rice, C., MacCormack, T., Stewart, J. M., & Dugourd, D. (2018). Abstract 2891: Molecular profiling of hormone-resistant prostate cancer cells with TRPV6 oncochannel knockout/knockdown. *Cancer research, 78*(13 Supplement), 2891.

Madaro, L., Pelle, A., Nicoletti, C., Crupi, A., Marrocco, V., Bossi, G., . . . Bouché, M. (2012). PKC theta ablation improves healing in a mouse model of muscular dystrophy. *PloS one, 7*(2), e31515-e31515.

Matsuda, N., Sato, S., Shiba, K., Okatsu, K., Saisho, K., Gautier, C. A., . . . Tanaka, K. (2010). PINK1 stabilized by mitochondrial depolarization recruits Parkin to damaged mitochondria and activates latent Parkin for mitophagy. *The Journal of cell biology, 189*(2), 211-221.

Micheva-Viteva, S. N., Shou, Y., Ganguly, K., Wu, T. H., & Hong-Geller, E. (2017). PKC-η-MARCKS Signaling Promotes Intracellular Survival of Unopsonized

Burkholderia thailandensis. *Frontiers in cellular and infection microbiology*, *7*, 231-231.

Mochida, K., Oikawa, Y., Kimura, Y., Kirisako, H., Hirano, H., Ohsumi, Y., & Nakatogawa, H. (2015). Receptor-mediated selective autophagy degrades the endoplasmic reticulum and the nucleus. *Nature*, *522*, 359.

Müller, O., Sattler, T., Flötenmeyer, M., Schwarz, H., Plattner, H., & Mayer, A. (2000). Autophagic Tubes. *The Journal of Cell Biology*, *151*(3), 519.

Nakatogawa, H., Ichimura, Y., & Ohsumi, Y. (2007). Atg8, a ubiquitin-like protein required for autophagosome formation, mediates membrane tethering and hemifusion. *Cell*, *130*(1), 165-178.

Narendra, D., Tanaka, A., Suen, D.-F., & Youle, R. J. (2008). Parkin is recruited selectively to impaired mitochondria and promotes their autophagy. *The Journal of cell biology*, *183*(5), 795-803.

Nath, S., Dancourt, J., Shteyn, V., Puente, G., Fong, W. M., Nag, S., . . . Melia, T. J. (2014). Lipidation of the LC3/GABARAP family of autophagy proteins relies on a membrane-curvature-sensing domain in Atg3. *Nature cell biology*, *16*(5), 415.

Newton, A. C. (1995). Protein kinase C: structure, function, and regulation. *Journal of biological chemistry*, *270*(48), 28495-28498.

Niemeyer, B. A., Bergs, C., Wissenbach, U., Flockerzi, V., & Trost, C. (2001). Competitive regulation of CaT-like-mediated Ca²⁺ entry by protein kinase C and calmodulin. *Proceedings of the National Academy of Sciences*, *98*(6), 3600.

Obara, K., Noda, T., Niimi, K., & Ohsumi, Y. (2008). Transport of phosphatidylinositol 3-phosphate into the vacuole via autophagic membranes in Saccharomyces cerevisiae. *Genes to Cells*, *13*(6), 537-547.

Park, C., Suh, Y., & Cuervo, A. M. (2015). Regulated degradation of Chk1 by chaperone-mediated autophagy in response to DNA damage. *Nature communications*, *6*, 6823-6823.

Pattingre, S., & Levine, B. (2006). Bcl-2 inhibition of autophagy: a new route to cancer? *Cancer research*, *66*(6), 2885-2888.

Qu, L., Li, G., Xia, D., Hongdu, B., Xu, C., Lin, X., & Chen, Y. (2016). PRKCI negatively regulates autophagy via PIK3CA/AKT–MTOR signaling. *Biochemical and Biophysical Research Communications*, *470*(2), 306-312.

Quack, I., Woznowski, M., Potthoff, S. A., Palmer, R., Königshausen, E., Sivritas, S., . . . Sellin, L. (2011). PKC alpha mediates beta-arrestin2-dependent nephrin endocytosis in hyperglycemia. *The Journal of biological chemistry*, *286*(15), 12959-12970.

Ramos, K., Reyes-Reyes, E., & Nanez, A. (2018). Overview of Receptor Systems.

Raphaël, M., Lehen'kyi, V. y., Vandenberghe, M., Beck, B., Khalimonchyk, S., Vanden Abeele, F., . . . Prevarskaya, N. (2014). TRPV6 calcium channel translocates to the plasma membrane via Orai1-mediated mechanism and controls cancer cell survival. *Proceedings of the National Academy of Sciences, 111*(37), E3870.

Rimessi, A., Pavan, C., Ioannidi, E., Nigro, F., Morganti, C., Brugnoli, A., . . . Pinton, P. (2017). Protein Kinase C β: a New Target Therapy to Prevent the Long-Term Atypical Antipsychotic-Induced Weight Gain. *Neuropsychopharmacology : official publication of the American College of Neuropsychopharmacology, 42*(7), 1491-1501.

Russo, R., Cattaneo, F., Lippiello, P., Cristiano, C., Zurlo, F., Castaldo, M., . . . Miniaci, M. C. (2018). Motor coordination and synaptic plasticity deficits are associated with increased cerebellar activity of NADPH oxidase, CAMKII, and PKC at preplaque stage in the TgCRND8 mouse model of Alzheimer's disease. *Neurobiology of Aging, 68*, 123-133.

Sajan, M. P., Hansen, B. C., Higgs, M. G., Kahn, C. R., Braun, U., Leitges, M., . . . Farese, R. V. (2018). Atypical PKC, PKCλ/ι, activates β-secretase and increases Aβ1–40/42 and phospho-tau in mouse brain and isolated neuronal cells, and may link hyperinsulinemia and other aPKC activators to development of pathological and memory abnormalities in Alzheimer's disease. *Neurobiology of Aging, 61*, 225-237.

Sanna, M. D., Quattrone, A., Ghelardini, C., & Galeotti, N. (2014). PKC-mediated HuD–GAP43 pathway activation in a mouse model of antiretroviral painful neuropathy. *Pharmacological Research, 81*, 44-53.

Schneider, J. L., Villarroya, J., Diaz-Carretero, A., Patel, B., Urbanska, A. M., Thi, M. M., . . . Cuervo, A. M. (2015). Loss of hepatic chaperone-mediated autophagy accelerates proteostasis failure in aging. *Aging cell, 14*(2), 249-264.

Schultz, A., Ling, M., & Larsson, C. (2004). Identification of an amino acid residue in the protein kinase C C1b domain crucial for its localization to the Golgi network. *Journal of Biological Chemistry, 279*(30), 31750-31760.

Seo, A. Y., Lau, P.-W., Feliciano, D., Sengupta, P., Gros, M. A. L., Cinquin, B., . . . Lippincott-Schwartz, J. (2017). AMPK and vacuole-associated Atg14p orchestrate μ-lipophagy for energy production and long-term survival under glucose starvation. *eLife, 6*, e21690.

Smith, R. E., & Farquhar, M. G. (1966). Lysosome function in the regulation of the secretory process in cells of the anterior pituitary gland. *The Journal of cell biology, 31*(2), 319-347.

So, K.-Y., & Oh, S.-H. (2016). Cadmium-induced heme-oxygenase-1 expression plays dual roles in autophagy and apoptosis and is regulated by both PKC-δ and PKB/Akt activation in NRK52E kidney cells. *Toxicology, 370*, 49-59.

Song, H., Dong, M., Zhou, J., Sheng, W., Li, X., & Gao, W. (2018). Expression and prognostic significance of TRPV6 in the development and progression of pancreatic cancer. *Oncology reports, 39*(3), 1432-1440.

Spitaler, M., & Cantrell, D. A. (2004). Protein kinase C and beyond. *Nature immunology, 5*(8), 785.

Steinberg, S. F. (2008). Structural basis of protein kinase C isoform function. *Physiological reviews, 88*(4), 1341-1378.

Strappazzon, F., Nazio, F., Corrado, M., Cianfanelli, V., Romagnoli, A., Fimia, G. M., . . . Cecconi, F. (2015). AMBRA1 is able to induce mitophagy via LC3 binding, regardless of PARKIN and p62/SQSTM1. *Cell death and differentiation, 22*(3), 419-432.

Tait, S. W. G., & Green, D. R. (2012). Mitochondria and cell signalling. *Journal of cell science, 125*(Pt 4), 807-815.

Tasdemir, E., Maiuri, M. C., Galluzzi, L., Vitale, I., Djavaheri-Mergny, M., D'Amelio, M., . . . Kroemer, G. (2008). Regulation of autophagy by cytoplasmic p53. *Nature Cell Biology, 10*(6), 676-687.

Tasdemir, E., Maiuri, M. C., Morselli, E., Criollo, A., D'Amelio, M., Djavaheri-Mergny, M., . . . Kroemer, G. (2008). A dual role of p53 in the control of autophagy. *Autophagy, 4*(6), 810-814.

Toton, E., Romaniuk, A., Konieczna, N., Hofmann, J., Barciszewski, J., & Rybczynska, M. (2018). Impact of PKCε downregulation on autophagy in glioblastoma cells. *BMC cancer, 18*(1), 185-185.

Uttenweiler, A., Schwarz, H., & Mayer, A. (2005). Microautophagic vacuole invagination requires calmodulin in a Ca2+-independent function. *Journal of Biological Chemistry, 280*(39), 33289-33297.

Valdor, R., Mocholi, E., Botbol, Y., Guerrero-Ros, I., Chandra, D., Koga, H., . . . Macian, F. (2014). Chaperone-mediated autophagy regulates T cell responses through targeted degradation of negative regulators of T cell activation. *Nature immunology, 15*(11), 1046-1054.

van Zutphen, T., Todde, V., de Boer, R., Kreim, M., Hofbauer, H. F., Wolinski, H., . . . Kohlwein, S. D. (2014). Lipid droplet autophagy in the yeast Saccharomyces cerevisiae. *Molecular biology of the cell, 25*(2), 290-301.

https://www.ncbi.nlm.nih.gov/pmc/articles/PMC3890349/.

Walther, T. C., & Farese, R. V., Jr. (2012). Lipid droplets and cellular lipid metabolism. *Annual review of biochemistry, 81*, 687-714.

Wang, B.-S., Yang, Y., Lu, H.-Z., Shang, L., Zhang, Y., Hao, J.-J., . . . Wang, M.-R. (2014). Inhibition of atypical protein kinase Cι induces apoptosis through autophagic degradation of β-catenin in esophageal cancer cells. *Molecular Carcinogenesis, 53*(7), 514-525.

Wang, B.-S., Yang, Y., Yang, H., Liu, Y.-Z., Hao, J.-J., Zhang, Y., . . . Wang, M.-R. (2013). PKCι counteracts oxidative stress by regulating Hsc70 in an esophageal cancer cell line. *Cell stress & chaperones, 18*(3), 359-366.

Wang, C., Wang, H., Zhang, D., Luo, W., Liu, R., Xu, D., . . . Liu, Z. (2018). Phosphorylation of ULK1 affects autophagosome fusion and links chaperone-mediated autophagy to macroautophagy. *Nature Communications, 9*(1), 3492.

Wang, F., Xu, C., Reece, E. A., Li, X., Wu, Y., Harman, C., . . . Yang, P. (2017). Protein kinase C-alpha suppresses autophagy and induces neural tube defects via miR-129-2 in diabetic pregnancy. *Nature Communications, 8*, 15182.

Wang, G.-S., Kuyumcu-Martinez, M. N., Sarma, S., Mathur, N., Wehrens, X. H. T., & Cooper, T. A. (2009). PKC inhibition ameliorates the cardiac phenotype in a mouse model of myotonic dystrophy type 1. *The Journal of clinical investigation, 119*(12), 3797-3806.

Wang, K., & Klionsky, D. J. (2011). Mitochondria removal by autophagy. *Autophagy, 7*(3), 297-300.

Wong, V. K. W., Zeng, W., Chen, J., Yao, X. J., Leung, E. L. H., Wang, Q. Q., . . . Law, B. Y. K. (2017). Tetrandrine, an Activator of Autophagy, Induces Autophagic Cell Death via PKC-α Inhibition and mTOR-Dependent Mechanisms. *Frontiers in pharmacology, 8*, 351-351.

Xie, Z., & Klionsky, D. J. (2007). Autophagosome formation: core machinery and adaptations. *Nature cell biology, 9*(10), 1102.

Xue, X., Ren, J., Sun, X., Gui, Y., Feng, Y., Shu, B., . . . Dai, C. (2018). Protein kinase Cα drives fibroblast activation and kidney fibrosis by stimulating autophagic flux. *The Journal of biological chemistry, 293*(28), 11119-11130.

Yamano, K., & Youle, R. J. (2013). PINK1 is degraded through the N-end rule pathway. *Autophagy, 9*(11), 1758-1769.

Yan, R., Niu, C.-Y., & Tian, Y. (2018). Roles of Autophagy and Protein Kinase C-epsilon in Lipid Metabolism of Nonalcoholic Fatty Liver Cell Models. *Archives of Medical Research, 49*(6), 381-390.

Yang, Q., Langston, J. C., Tang, Y., Kiani, M. F., & Kilpatrick, L. E. (2019). The Role of Tyrosine Phosphorylation of Protein Kinase C Delta in Infection and Inflammation. *International journal of molecular sciences, 20*(6), 1498.

Young, A. R. J., Chan, E. Y. W., Hu, X. W., Köchl, R., Crawshaw, S. G., High, S., . . . Tooze, S. A. (2006). Starvation and ULK1-dependent cycling of mammalian Atg9 between the TGN and endosomes. *Journal of Cell Science, 119*(18), 3888.

Zhang, D., Han, S., Wang, S., Luo, Y., Zhao, L., & Li, J. (2017). cPKCγ-mediated down-regulation of UCHL1 alleviates ischaemic neuronal injuries by decreasing autophagy via ERK-mTOR pathway. *Journal of cellular and molecular medicine, 21*(12), 3641-3657.

Zhang, D., Pan, J., Xiang, X., Liu, Y., Dong, G., Livingston, M. J., . . . Dong, Z. (2017a). Protein Kinase Cδ Suppresses Autophagy to Induce Kidney Cell Apoptosis in Cisplatin Nephrotoxicity. *Journal of the American Society of Nephrology, 28*(4), 1131-1144.

Zhang, D., Pan, J., Xiang, X., Liu, Y., Dong, G., Livingston, M. J., . . . Dong, Z. (2017b). Protein Kinase Cδ Suppresses Autophagy to Induce Kidney Cell Apoptosis in Cisplatin Nephrotoxicity. *Journal of the American Society of Nephrology : JASN, 28*(4), 1131-1144.

PUBLICATIONS AND PRESANTATIONS

Kaleli H.N., Ozer E., Kaya V.O., Kutlu O. Protein Kinase C Isozymes and Autophagy During Neurodegenerative Disease Progression (2019) **(under revision)**

Kutlu O., **Kaleli H.N.**, Ozer E., Molecular Pathogenesis of Nonalcoholic Steatohepatitis (NASH) Related Hepatocellular Carcinoma, Canadian Journal of Gastroenterology and Hepatology, doi.org/10.1155/2018/8543763

Kaleli H.N., Kaya V.O., Yedier-Bayram O., Kilic S., Onal G., Yuce A., Dokmeci S., Gozuacik D., Kutlu O., (2019) Reverse Activation of Defective Autophagy Mechanism Might Be an Alternative Approach for Gaucher Disease Therapy, 13th European Working Group on Gaucher Disease Congress (EWGGD 2019)**,** Clermont-Ferrand, France

Ozer O., **Kaleli H.N.**, Taskın E., Kutlu O., (2019) Association Between *PNPLA3* rs738409 polymorphism with Autophagy and Non-alcoholic Steatohepatitis (NASH),3rd Cukurova Hepatocellular Carcinoma Congress, Turkey

Kaleli H.N., Ozer E., Yedier-Bayram O., Kilic S., Dokmeci S., Gozuacik D., Kutlu O. (2018) Identification of Novel Targets for The Role of PKC Isozymes on The Regulation of Autophagy, 6th International Congress of the Molecular Biology Association of Turkey